DOCTORATE THESIS

Angular dynamics of small particles in fluids

JONAS EINARSSON

Department of Physics
University of Gothenburg
Göteborg, Sweden 2015

Angular dynamics of small particles in fluids
Jonas Einarsson
ISBN 978-91-628-9656-0 (PDF)
ISBN 978-91-628-9657-7 (Print)

This thesis is electronically published, available at
http://hdl.handle.net/2077/40830

Department of Physics
University of Gothenburg
SE-412 96 Göteborg
Sweden
Telephone: +46 (0)31-786 00 00

Front cover: Illustration of ellipsoidal particle tumbling in a shear flow.
Flipbooks: Ellipsoidal particles rotating in a simple shear flow.
Odd pages: Symmetric particle with major aspect ratio $\lambda = 7$ and minor aspect ratio $\kappa = 1$. *Even pages:* Slightly asymmetric particle with $\lambda = 7$ and $\kappa = 1.2$. Their trajectories are qualitatively different despite the very slight asymmetry. See Section 3.5 for further explanation.

Printed by Kompendiet
Göteborg, Sweden 2015

ABSTRACT

This thesis concerns the angular motion of small particles suspended in fluid flows. A small particle experiences a hydrodynamic torque due to the local fluid velocity, and this torque leads to rotational motion. When inertial effects are negligible the torque on an ellipsoidal particle is given by Jeffery's theory [JEFFERY, G. B. *Proc. R. Soc. Lond. A* **102**, 161–179 (1922)]. In this thesis and the appended papers I describe three studies that all relate to this well-known result.

First, we derive an effective equation of motion for the orientation of a spheroid in a simple shear flow, valid for small values of the shear Reynolds number $\mathrm{Re}_s = sa^2/\nu$, where s is the shear rate, a the particle size and ν the kinematic viscosity of the suspending fluid. In absence of inertia the equation of motion has infinitely many periodic solutions, the 'Jeffery orbits'. We show how this degeneracy is lifted by the effects of inertia.

Second, we describe experimental observations of the orientational dynamics of asymmetric particles advected in a microchannel. We record several trajectories with each particle by resetting the initial condition with an optical trap. We find that the dynamics depend sensitively on both particle shape and initial conditions. This confirms earlier theoretical results, which are also described in this thesis.

Third, we discuss the angular dynamics of axisymmetric particles in turbulent and random flow. In these flows the statistical averages of the angular dynamical quantities depend crucially on the intricate correlations between the particle orientation, angular velocity, and the flow vorticity relative to the principal straining directions of the fluid flow. We illustrate this by direct numerical simulation, experimental measurements and statistical model calculations.

Finally, this thesis contains an introduction to the field aimed at new students, as well as an accessible popular science introduction to low Reynolds particle dynamics.

List of papers

This thesis builds on the scientific work in the following papers:

Paper A
Einarsson, J, Candelier, F, Lundell, F, Angilella, J. R & Mehlig, B 2015 Effect of weak fluid inertia upon Jeffery orbits. *Physical Review E* **91** (4), 041002.

Paper B
Candelier, F, Einarsson, J, Lundell, F, Mehlig, B & Angilella, J. R 2015 Role of inertia for the rotation of a nearly spherical particle in a general linear flow. *Physical Review E* **91** (5), 053023.

Paper C
Einarsson, J, Candelier, F, Lundell, F, Angilella, J. R & Mehlig, B 2015 Rotation of a spheroid in a simple shear at small Reynolds number. *Physics of Fluids* **27** (6), 063301.

Paper D
Rosen T, Einarsson, J, Nordmark, A, Aidun, C. K, Lundell, F & Mehlig, B 2015 Numerical analysis of the angular motion of a neutrally buoyant spheroid in shear flow at small Reynolds numbers. *Physical Review E (in review).* arXiv 1508.04976.

Paper E
Einarsson, J, Mihiretie, B. M, Laas, A, Ankardal, S, Angilella, J. R, Hanstorp, D, & Mehlig, B 2015 Tumbling of asymmetric microrods in a microchannel flow. *Physics of Fluids (in review).* arXiv 1503.03023

Paper F
Byron, M, Einarsson, J, Gustavsson, K, Voth, G, Mehlig, B & Variano, E 2015 Shape-dependence of particle rotation in isotropic turbulence. *Physics of Fluids* **27** (3), 035101.

My contributions

My contributions to the appended publications are:

Papers A-D

I devised and performed the main calculation (presented in Paper C) valid for arbitrary aspect ratio. I performed the stability analysis in Paper D. I wrote Paper C in collaboration with BM, and I took active part in writing of Papers A, B and D.

Paper E

I took part in designing the experiment and the data analysis. I did the theory together with BM, in particular the reversal symmetry arguments and Eq. (2). I wrote Sections I & II, and took active part in editing of the entire manuscript.

Paper F

I computed the DNS results and took active part in interpreting the results of experiments, DNS and random models. I wrote most of Sec. IV and App. A, and took active part in writing the rest of the paper.

Earlier work

The following publications were part of my Licentiate thesis [1]:

Gustavsson, K, Einarsson, J & Mehlig, B 2014 Tumbling of small axisymmetric particles in random and turbulent flows. *Physical Review Letters* **112** (1), 014501.

Einarsson, J, Angilella, J. R & Mehlig, B 2014 Orientational dynamics of weakly inertial axisymmetric particles in steady viscous flows. *Physica D: Nonlinear Phenomena* **278–279**, 79–85.

Einarsson, J, Johansson, A, Mahato, S. K, Mishra, Y. N, Angilella, J. R, Hanstorp, D & Mehlig, B 2013 Periodic and aperiodic tumbling of microrods advected in a microchannel flow. *Acta Mechanica* **224** (10), 2281–2289.

CONTENTS

Abstract

List of papers

My contributions

Earlier work

Contents

I Introduction **1**

1 Motivation **2**

2 Background **5**
2.1 Our field of study: particles in flows 5

3 Prerequisite concepts **11**
3.1 Fluid mechanics 12
3.2 Effective equations of motion 15
3.3 The Stokes approximation 18
3.4 Simple shear flow 20
3.5 The Jeffery equation and its solutions 22

II My work **43**

4 Effects of inertia **43**
4.1 History of problem 44
4.2 Results 46

5 Measurements of asymmetric rods **51**
5.1 Overview 51

6 Rotation rates of particles in turbulence **52**

7 Closing words **54**
7.1 Discussion of results 55
7.2 Outlook 56

Acknowledgements **61**

A Triaxial particle in a linear flow **69**

III Papers **73**

PART I
INTRODUCTION

This thesis is about *effective equations of motion* for solid particles suspended in fluid flows. In all but the simplest cases we are unable to directly compute the forces acting on a solid particle from first principles. The fundamental equations of fluid mechanics are too complicated, and even finding a numerical approximation with a computer is often too expensive.

But if we limit our scope to a particular physical situation, we may exploit its particular properties to simplify the calculations. With these simplifications we may find an effective equation governing the motion of the suspended particles. The effective equation is simpler, and therefore more useful, than the fundamental equations. The price for the simplicity is that they apply only within the limited scope. In this thesis we consider *small* particles. I will make a precise definition of what small means later. For now think of small as the plankton in the oceans, not the shark, or the mist droplets in the clouds, not an airplane.

The effective equations of motion are used as building blocks in higher-level modeling. For example the effective force on a small sphere becomes a building block in a model of the droplets in a rain cloud, and the effective torque on a spheroid is used to model the order of fibers in a paper-making machine.

The technical centerpiece of this thesis is the calculation of an effective equation of motion, starting from the fundamental equations. This effective equation describes the rotation of a spheroid which is small, but finite. The motion of a finite particle is affected by inertia, and so is the motion of the surrounding fluid. The inertia affects the forces and torques acting on the particle. These effects are captured in our calculation. It is described in detail in Section 4 in Part II, and the appended Papers A-D.

The new effective equation generalises aspects of an earlier effective equation: the Jeffery equation [2], which is valid for truly small particles that are not affected by inertia. In addition to this project I have also worked on two other projects which involve the Jeffery equation (Papers E & F.)

Disposition of this thesis

The remainder of this thesis consists of an extended summary, and the appended papers.

You are now reading Part I, which continues in Section 1 with a motivation for our research. In Section 2 I attempt to introduce our research to a reader without a strong technical background. Perhaps the reader is a new student, or a curious uncle of mine. But I hope that also an experienced reader may enjoy the text. Section 3 is a technical introduction to the prerequisite concepts needed to understand this thesis. In particular I discuss the Jeffery equation and its solutions in some detail. Some material in Part I is adapted and revised from my Licentiate thesis [1].

Part II is where I present the original research contained in the appended papers. I give an "executive summary" of each project, including the context of the questions and the main results.

Part III consists of reprints of the Papers A-F.

1 Motivation

The motion of small particles suspended in fluid flows is a fundamental research topic of interest in many branches of science, as well as for technical applications. In some cases it is the actual motion of the particles that is of interest. For example, in the atmospheric sciences the collisions and aggregation of small drops are important to the formation of rain [3]. Similarly, in astronomy it is believed that the collisions of small dust grains lead eventually to the formation of planets in the accretion disk around a star [4]. Another example is in marine biology, where the dynamics of small planktonic organisms swirled around by the ocean is fundamental in understanding their feeding and mating patterns [5].

In other contexts the motion of the individual particle is of lesser interest. Instead its effects on the suspending fluid is the topic of study. The properties of so-called complex fluids, meaning fluids with suspended particles, are studied in the field of rheology. For instance, the "ketchup effect" (where ketchup is stuck in the bottle, and nothing happens, and then suddenly all the ketchup pours out at once, only to solidify again on the plate) exists because of how all the microscopic particles suspended in the liquid orient themselves

[6]. On a more serious note, the similarly sudden onset of landslides in clay soils is related to the complex fluid of water and clay particles [7]. A fundamental question in rheology is how to relate the microscopic motion of the suspended particles to the macroscopic behaviour of the complex fluid.

In many circumstances it is important to consider the non-spherical shape of particles, and how they are oriented. For instance, the ash clouds from volcanic eruptions play an important role in the radiation budget of our planet, and therefore its climate [8]. The ash particles are non-spherical [9], and their shapes and orientations influence how light and energy is absorbed in the volcanic cloud [10]. Similarly, the orientation of non-spherical plankton influences the light propagation through the upper layers of the oceans, determining to which depth life-supporting photosynthesis is possible [11].

Despite their diversity, all the above examples share a basis in a fundamental question. How do particles respond to a given flow, and how does the flow in return respond to the presence of particles? The underlying goal of our research is to find an answer to this fundamental question. But the mathematics of fluid dynamics have challenged physicists and mathematicians alike for several hundred years. Before moving on to the description of my work, I allow myself to digress into the story of a seemingly innocent question: what is the drag force on a perfect sphere moving with constant velocity through a still fluid?

Until the early 19th century the prevailing theory was the following: a moving sphere drags along some of the surrounding fluid in its motion, and the force upon the sphere is equal to the force required to drag along the extra weight. The force must then be dependent on the weight, or more precisely the density, of the fluid. But in 1829, Captain Sabine of the Royal Artillery performed detailed experiments with a pendulum in different gases [12]. By observing the attenuation of the pendulum motion in both hydrogen gas and in air, he concluded beyond doubt that the damping force on the pendulum is not proportional to the density of the surrounding gas - there has to be another force.

It was George Gabriel Stokes who first computed the force on a *slowly moving* sphere due to the internal friction of the fluid [13]. He found that the force depends on the "index of friction", which we today know as the kinematic viscosity of a fluid. From his calculation, Stokes immediately concluded that "the apparent suspension of the clouds is mainly due to the internal friction of air" [13].

The *Stokes drag force* remains a great success, and it correctly predicts the forces for slowly moving particles. But the question of how to correctly amend the Stokes drag force to account for slightly faster motion turned out to be surprisingly hard. The correction took around a century of hard work, and the invention of a new branch of mathematics [14]. If we dare ask how to properly calculate the drag force on a particle moving quickly, in a curved path, and in a fluid which itself moves, the answer is still debated.

Meanwhile, the Stokes theory for slow motion has been extended to include both forces and torques on particles of any conceivable shape [2, 15, 16]. Much of modern research on particles in fluid flows still rely directly on these well-known results.

In general, the fundamental equations of fluid mechanics, the Navier-Stokes equations, seem to describe the motion of fluids. But applying them requires tremendous efforts due to their sheer complexity. Today, a modern supercomputer can produce an approximate solution for some simplified cases, like a cubic meter of moderately turbulent air without particles. But many interesting problems, such as a real rain cloud with drops, are far out of reach for any computer in any foreseeable future.

One aim of theoretical fluid mechanics is to derive new, simpler, equations of motion to use in place of the fundamental equations. This is in essence what Stokes did in 1851 for slowly moving spheres. But the price of simplification is the loss of generality. Every new physical situation potentially requires a new equation. And each new equation has to be tested against experiments and direct numerical solution of the general equations.

In this thesis I first present a derivation (Papers A-C) and validation (Paper D) of an effective equation of motion for the orientation of a spheroid in a simple shear flow. This equation of motion takes one step beyond the Stokes approximation of slow movements, at the expense of being valid precisely only for the simple shear flow. Why this trade-off is worthwhile is explained in this thesis. Secondly, the two remaining papers appended to this thesis involve the Stokes (Jeffery [2]) approximation for the angular motion of ellipsoids in linear flows. Paper E is an experimental verification of the predicted angular motions in shear flow. Paper F discusses the rotations of axisymmetric particles in turbulent flows.

2 Background

Every now and then I get the question "what is it you do, anyway?" Often enough the question is posed out of sheer politeness, and I can simply say "Physics! Tiny particles, like plankton, they tumble in the oceans, and stuff." But sometimes the question is sincere, and I find it quite challenging to explain what I do. I may say that we calculate how non-spherical particles rotate in flows. But that is comparable to if I was designing a gearbox, and said that I work with cars. It is true, but not very helpful.

The following is an attempt at a description which is readable and not too complicated, but still complicated enough to get a glimpse of the physics.

2.1 Our field of study: particles in flows

Where do particles go when I put them into a flow? Which way do they face? How fast do they spin? These are all valid questions, but they are unspecific. Their answers depend on whether the particle is an aircraft or a grain of particulate carbon soot, and whether the fluid is air or water.

I will start with an elaboration on fluid physics, move to the question why we consider rigid particles specifically, then say something about the forces acting on the particles. This will naturally lead us to why we must consider "small" particles, which is not obvious from the outset. But let's start from the beginning.

Fluids

Many physical systems around us are fluids. The air we breathe, the water we drink, the blood in our veins are all fluids. As a working definition we can think of a fluid as a system where the constituent molecules move around more or less freely. Sometimes they interact with each other and exchange some energy. These interactions give rise to what you perceive as friction. You know that syrup has more friction than water: if you pull a spoon through syrup, more of your energy is expended than if you were to pull the spoon through water. The *viscosity* of a fluid is a measure of how often and how violently the molecules interact, and we say that syrup has higher viscosity than water. Now, it gets interesting when something else, for example a drop

of oil or a particle, is added to the fluid. Consider dripping a drop of oil into water. Then what happens depends on how the water molecules interact with the oil molecules. As you probably have experienced, oil molecules prefer to stick together. Therefore the oil concentrates into a drop where as many oil molecules as possible may be neighbours with other oil molecules.

But so far, the above is a very qualitative, and you may rightly say naive, description of what happens. One could say that a fundamental problem of fluid physics is to figure out where all the different molecules go. From the detailed knowledge of every molecule we may proceed to deduce where the oil drop goes, and how fast, or if it perhaps breaks up, or maybe merges with another drop. However, making something useful out of this molecular picture is very difficult. Just consider that in one litre of water there are about 10^{25} molecules (that is a one followed by 25 zeroes). In fact, we are not even particularly interested in the specific details of every molecule. We are interested in the macroscopic, observable world that is built up from all these molecules. Therefore this thesis is not at all concerned with the detailed motion of molecules, but I still wanted to start with this picture because sometimes it becomes important to remember the microscopic origin of the macroscopic motion.

Fluid dynamics

Fluid dynamics is the the discipline studying the macroscopic properties and motion of fluids. Some typical quantities studied there are the fluid velocity and pressure. We can think of the velocity at a certain position in the fluid as the average velocity of all the molecules at that point. The pressure is the force per area an object in contact with the fluid experiences, due to the constant bombardment of molecules. Think for example of the forces in a bottle of soda. There are well-known equations called the Navier-Stokes equations that tell us the velocity and pressure at every point in space and time, provided that we can solve them. You can see them in Eq. (3.7) on p. 13. We will soon return to how this helps us, but first we must restrict ourselves to avoid a difficult hurdle.

Recall our example of a drop of oil in water. The switch from a molecular view to a fluid dynamical view presents a new problem: if we do not keep track of every molecule, we instead have to keep track of which points in space contain oil and which contain water. A boundary surface separates

the two materials, and this boundary can deform over time as the oil drop changes shape. This sounds very complicated. Indeed, drop dynamics is a topic of its own, which this thesis does not intend to cover. Instead, this thesis concerns *rigid particles*.

Rigid bodies

A rigid body in physics is an object whose configuration can be described by the position of one point (usually the center-of-mass) and the rotation of the body around that point. Simply put: it cannot deform. The dynamics of a rigid body is described by Newton's laws. In particular, the center-of-mass motion is described by Newton's second law: the force $\boldsymbol{F}$ on a body equals its mass m times its acceleration $\boldsymbol{a}$,

$$\boldsymbol{F} = m\boldsymbol{a}.$$

The above equation describes the movement of the center-of-mass, and there is a corresponding law for the rotation. Since this thesis concerns *orientational dynamics* of particles, here is Newton's law for the rotation of a rigid body:

$$\boldsymbol{T} = \mathbb{I}\boldsymbol{\alpha}.$$

It says that the torque $\boldsymbol{T}$ on a rigid body equals its moment of inertia $\mathbb{I}$ (that's like the mass for rotations) times its angular acceleration $\boldsymbol{\alpha}$, The two equations above are deceivingly simple-looking, but their solutions contain full knowledge of the motion of a rigid body. I state the equations here only to draw a conclusion: in order to extract all the information about the motion of a particle, we need to know both the force and the torque acting on the particle at all times.

There are many kinds of forces which can potentially act on a particle. For example there is gravity if the particle is heavy, or magnetic forces if the particle is magnetic. But for now we consider the forces on a particle due to the surrounding fluid, so called hydrodynamic forces. In everyday terms the hydrodynamic force is the drag, as experienced by the spoon you pull through syrup. Uneven drag over a body may also result in a hydrodynamic torque. For instance, turbulent air striking the wings of an aircraft will induce a torque which you feel as a rotational acceleration while the pilot compensates.

Hydrodynamic forces

In order to find out what the force on a particle is, we need to know how the fluid around the particle behaves. And for that, we need to solve the Navier-Stokes equations of fluid dynamics around the particle. We imagine the fluid in some environment (in lingo: "boundary conditions"), for example the air in a cloud, or liquid soap in a small pipe. A solution of the equations tells us the velocity and pressure of the fluid at any given point in space at any given time. If we have a solution, there is a mathematical recipe for how to extract the resulting forces and torques on a particle in the fluid.

The problem is that we cannot solve the equations. Not only are we unable to find solutions as mathematical formulas – in many cases we can not even find numerical solutions using a supercomputer. For example, computing the motion of the air in a cloud is utterly out of reach with any computer we can currently imagine. Before moving on to how we find the force on a particle, I'll digress on the topic of numerical solutions.

From time to time I get the question why we struggle with difficult mathematical work, why not just "run it through the computer?" An answer to this question is that a numerical computer solution is like an experiment: it will give you the numbers for a particular case, but not necessarily any understanding of why. Conversely, we may extract physical understanding from the equations, even if we cannot solve them in general. It is the understanding of the underlying physics that enables us to simplify the equations until it is practical to solve them. This requires knowledge of which particular details may be neglected, and which details are crucial to keep track of. And indeed, the meteorologists now have methods of simulating the flows of air in the atmosphere, despite the fact that we cannot solve the exact equations. The trick is to ignore some parts of the equation dealing with very small motions, and spend the resources on describing the large eddies of the flow in so-called "Large Eddy Simulations".

At any rate, we wish to figure out what the forces on a rigid body in a fluid flow are. It is clear that some type of simplification has to be made, because we cannot solve the Navier-Stokes equations. The great simplification is embodied in the word *small* in the title of this thesis. The particles we consider are small. But how small is a small particle? The answer I have to give right away is a rather unsatisfactory "it depends". The smallness of the particle has to be relative to something else. This simple principle is

formalised by scientists, who discuss smallness in terms of *dimensionless numbers*. Because dimensionless numbers are very common in our work I will spend a few paragraphs to explain the basic idea.

Dimensionless numbers

In principle all physical quantities have some units. For example, the size of a particle has units of "length", and the speed of the particle has units of "length per time", which we write as length/time. Whenever we multiply or divide quantities with units, we also multiply or divide their units. For example dividing the length 20 m with the time 5 s gives the speed 4 m/s. Now suppose we divide the speed 4 m/s with the speed 2 m/s. The result is 2, without any units – they cancelled in the division.

The idea is that in order to determine if a quantity x_1 is "small" we have to divide it with another quantity x_2 of the same units. Then if the resulting dimensionless number x_1/x_2 is much smaller than 1, we say that x_1 is small, and implicitly mean *relative to* x_2. This concept seems simple enough. Let's apply it to particles moving in a fluid.

An example: the particle Reynolds number

Imagine stirring your cup of tea with a spoon. As you stir there is a wake behind the spoon, perhaps even a vortex is created if you are enthusiastic. When you stop stirring, the tea will splash about for a moment and then settle down because of its viscosity. If you stir vigorously, then stop suddenly and hold on to the spoon, you feel the force of the splashing fluid on the spoon. This continuing motion after you stopped forcing the fluid is due to the inertia of the fluid. Inertia means that things continue to move in their current direction, unless a force is applied. The inertia of the fluid is difficult to analyse mathematically, because the force on the spoon depends in a complicated fashion on how you stirred the tea in the past. To perform my calculation I want the inertia to be *small*. But small compared to what? How can I make a dimensionless number?

Imagine stirring with a spoon in syrup instead of tea. The wake behind the spoon relaxes quickly in the more viscous fluid. The viscous friction is the force which cancels the inertia. Viscous friction smears out any disturbances. Therefore we divide two times: the time it takes for viscosity to smear out

a disturbance over the size of the spoon (the *viscous time*), with the time it takes for the fluid to flow past the spoon:

$$\mathrm{Re_p} = \frac{\text{Viscous time}}{\text{Time for fluid to flow past the spoon}}.$$

This number is called the particle Reynolds number. It is small when inertia is not important. If the viscous time is short, a disturbance is smeared out before it is allowed to flow past the particle. This is similar to stirring syrup. But if the fluid flows past the particle before the viscosity can smear out the disturbances, the particle Reynolds number is larger, like in your cup of tea.

The mathematical expression for the particle Reynolds number is

$$\mathrm{Re_p} = \frac{u_0 a}{\nu},$$

where u_0 is the fluid velocity past the particle (units m/s), a is the particle size (units m), and ν is the viscosity (units m^2/s). This gives us three options to keep the effects of inertia small: consider slower flows, or smaller particles, or fluids with higher viscosity.

Recall the story about the Stokes drag in the very beginning of this thesis. When Stokes in 1851 called a particle "slowly moving", he meant exactly the condition that the particle is small, in the sense just described here. Among friends we often say "small particle", or "slowly moving", or "viscous flow", when we mean "small value of the particle Reynolds number." It is convenient, but less precise.

The reduction of three options into the value of a single number is an important insight. Instead of considering the effects of all three separate parameters, we can understand the physics by analysing a single dimensionless number. The dimensionless numbers tell us which physical quantities are important in relation to each other. In the example above, the actual size of the particle is not important – the size only matters in relation to the velocity and viscosity. All situations with the same particle Reynolds number are, in some sense, equivalent. This very fact is also what enables engineers to use scale models in wind tunnels. They know that to test a model of a suspension bridge in a wind tunnel, they must not use full-scale wind speeds, but instead a scaled down version of the wind. The dimensionless numbers reveal what scaling is appropriate to match the model bridge to real conditions.

Conclusion

We have discussed fluids, rigid particles, the Navier-Stokes equations and dimensionless numbers. If we add some mathematical rigor to the mix, you could soon have an undergraduate degree in fluid mechanics. But how does this connect to my research?

When we assume that there is no fluid inertia whatsoever, that is $\mathrm{Re}_\mathrm{p} = 0$, we enter the regime of the Stokes approximation. As explained in the introduction this approximation has been fantastically successful in predicting the forces and torques on particles in many situations. But for some special cases, the Stokes approximation does not lead to a definite answer. One of these cases is the rotation of a non-spherical particle in a so-called shear flow. Jeffery applied the Stokes approximation to this problem in 1922, and was disappointed to find that the answer is indeterminate. My contribution in this thesis is to amend the Stokes approximation for this particular case. The four Papers A-D explain the first effects of both fluid and particle inertia on the rotation of a non-spherical particle in shear flow.

During the course of this work, I have also worked with students and collegues on related problems. How does the particle rotate if we throw it into a turbulent fluid? Can we tune an experiment to match the Stokes approximation? These and many more questions are ongoing work, and we published some results in the Papers E & F.

3 Prerequisite concepts

In this section I introduce some basic concepts needed to understand my work in Part II of this thesis, and the appended papers. My aim is to start at the beginning, and as quickly as possible arrive at the knowledge particular to the field of orientational dynamics of non-spherical particles. The scope is therefore narrow, but deep. For a wider presentation of low-Reynolds hydrodynamics I refer to the books by Kim & Karrila [16] and Happel & Brenner [17].

3.1 Fluid mechanics

3.1.1 Fluid flows

In this thesis we only encounter so-called Newtonian and incompressible fluids. The hydrodynamic state of such a fluid is described by a flow velocity vector field $\boldsymbol{u}(\boldsymbol{x},t)$, and a scalar pressure field $p(\boldsymbol{x},t)$. The incompressible nature of the fluid implies that $\nabla\cdot\boldsymbol{u}=0$ everywhere. The fluid itself has two properties: its density ρ_f (kg/m^3), and its dynamic viscosity μ (kg/m·s). Sometimes it is convenient to refer to the kinematic viscosity $\nu=\mu/\rho_f$ (m^2/s).

The work presented in this thesis involves the flow gradients, because it is the gradients in the flow that give rise to the torque on a small particle. The spatial derivatives of the flow field $\boldsymbol{u}$ form a tensor $\mathbb{A}\equiv\nabla\boldsymbol{u}^{\mathrm{T}}$, because there are three vector components defined in three coordinates. The components of $\mathbb{A}$ in Cartesian coordinates are

$$A_{ij}=\frac{\partial u_i}{\partial x_j}. \tag{3.1}$$

In general the action of $\mathbb{A}$ is defined as the directional derivative in the direction of the unit vector $\hat{\boldsymbol{y}}$:

$$\mathbb{A}\hat{\boldsymbol{y}}=\lim_{\epsilon\to 0}\frac{\boldsymbol{u}(x+\epsilon\hat{\boldsymbol{y}},t)-\boldsymbol{u}(\boldsymbol{x},t)}{\epsilon}. \tag{3.2}$$

The incompressibility condition $\nabla\cdot\boldsymbol{u}=0$ transfers directly to the condition $\mathrm{Tr}\mathbb{A}=0$.

It is often convenient to decompose the gradient tensor $\mathbb{A}$ into its symmetric part $\mathbb{S}$ and anti-symmetric part $\mathbb{O}$, because they have separate physical interpretations. We write

$$\mathbb{A}=\mathbb{S}+\mathbb{O},\qquad \mathbb{S}=\frac{1}{2}\left(\mathbb{A}+\mathbb{A}^{\mathrm{T}}\right),\qquad \mathbb{O}=\frac{1}{2}\left(\mathbb{A}-\mathbb{A}^{\mathrm{T}}\right). \tag{3.3}$$

The symmetric part $\mathbb{S}$ is called the rate-of-strain tensor, and it describes the local rate of deformation of the flow. The anti-symmetric part $\mathbb{O}$ describes the local rotation of the flow and is related to the vorticity vector. The vorticity vector $\boldsymbol{\omega}_f$ of a flow $\boldsymbol{u}$ is defined by the curl $\boldsymbol{\omega}_f=\nabla\times\boldsymbol{u}$. The matrix $\mathbb{O}$ is related to the vorticity vector $\boldsymbol{\omega}_f$, because for any given vector $\boldsymbol{x}$

$$\mathbb{O}\boldsymbol{x}=\frac{1}{2}\boldsymbol{\omega}_f\times\boldsymbol{x}\equiv\boldsymbol{\Omega}\times\boldsymbol{x}. \tag{3.4}$$

The vector $\boldsymbol{\Omega} = \boldsymbol{\omega}_f/2$ is a common quantity in our calculations, and therefore is given its own symbol. For example, in absence of inertia the angular velocity of a sphere in a simple shear flow is exactly $\boldsymbol{\Omega}$. This is explained in detail in Section 3.5.

3.1.2 The Navier-Stokes equations

For a given physical situation the flow and pressure fields are determined by a Navier-Stokes problem. A Navier-Stokes problem for a Newtonian, incompressible fluid is fully specified by a momentum balance, the incompressibility condition and a set of boundary conditions.

Let us first derive the momentum equations. Consider the momentum balance in a volume $\mathscr{V}$ bounded by surface $\mathscr{S}$. These equations are Newton's $m\boldsymbol{a} = \boldsymbol{F}$ over a volume:

$$\frac{\partial}{\partial t}\int_{\mathscr{V}} \rho_f \boldsymbol{u}\,\mathrm{d}\mathscr{V} + \int_{\mathscr{S}} \rho_f \boldsymbol{u}(\boldsymbol{u}\cdot\mathrm{d}\mathscr{S}) = \int_{\mathscr{S}} \boldsymbol{\sigma}\cdot\mathrm{d}\mathscr{S} \tag{3.5}$$

The first term accounts for changing velocities in the bulk of the volume. The second term accounts for the momentum transfer across the boundary of the volume. The right hand side contains the forces acting on the surface of the volume. The stress tensor $\boldsymbol{\sigma}$ describes the force per unit area in the fluid, such that $\boldsymbol{\sigma}\cdot\boldsymbol{N}$ is the force per area on a surface with normal vector $\boldsymbol{N}$. A Newtonian fluid is modeled by $\boldsymbol{\sigma} = -p\mathbb{1} + 2\mu\mathbb{S}$, meaning that the forces arise in part from pressure, and in part from the viscous friction forces. This tensor is central in determining the forces on particle surfaces, too, as will be explained below.

We apply the divergence theorem to the surface integrals in Eq. (3.5) and find

$$\frac{\partial}{\partial t}\int_{\mathscr{V}} \rho_f \boldsymbol{u}\,\mathrm{d}\mathscr{V} + \int_{\mathscr{V}} \left[(\nabla\cdot\rho_f\boldsymbol{u})\boldsymbol{u} + (\rho_f\boldsymbol{u}\cdot\nabla)\boldsymbol{u}\right]\mathrm{d}\mathscr{V} = \int_{\mathscr{V}} \nabla\cdot\boldsymbol{\sigma}\,\mathrm{d}\mathscr{V}. \tag{3.6}$$

This equation holds point-wise, because the volume can be arbitrarily chosen. By using the incompressibility condition, we arrive at the Navier-Stokes equations for an incompressible fluid:

$$\rho_f\left(\frac{\partial}{\partial t}\boldsymbol{u} + (\boldsymbol{u}\cdot\nabla)\boldsymbol{u}\right) = \nabla\cdot\boldsymbol{\sigma}, \quad \nabla\cdot\boldsymbol{u} = 0, \quad \boldsymbol{\sigma} = -p\mathbb{1} + 2\mu\mathbb{S}. \tag{3.7}$$

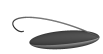

The boundary condition where the fluid meets a solid surface is the *no-slip condition*. This means that the fluid at the boundary has the same velocity as the boundary itself. When considering problems with a solid particle suspended in a fluid, the typical boundary condition is no-slip on the particle surface and that the flow relaxes to a prescribed background flow as the distance to the particle goes to infinity.

3.1.3 Forces on particles

Consider a background flow $\boldsymbol{u}^\infty(\boldsymbol{x}, y)$ without any particle present. We introduce a particle into the flow through the no-slip boundary conditions at the particle surface S. The particle center-of-mass moves along the trajectory $\boldsymbol{y}(t)$ (velocity $\dot{\boldsymbol{y}}$), and its orientation $\mathbb{R}(t)$ changes with angular velocity $\boldsymbol{\omega}(t)$. Far away from the particle, "at infinity", the fluid is not disturbed by the presence of the particle, and should be equal to $\boldsymbol{u}^\infty(\boldsymbol{x}, t)$:

$$\begin{aligned} \boldsymbol{u}(\boldsymbol{x}, t) &= \dot{\boldsymbol{y}} + \boldsymbol{\omega} \times (\boldsymbol{x} - \boldsymbol{y}), & \boldsymbol{x} &\in S(\boldsymbol{y}, \mathbb{R}). \\ \boldsymbol{u}(\boldsymbol{x}, t) &= \boldsymbol{u}^\infty(\boldsymbol{x}, t), & |\boldsymbol{x} - \boldsymbol{y}| &\to \infty . \end{aligned} \tag{3.8}$$

As explained above, the hydrodynamic force on a surface in the fluid is determined by integrating the fluid stress tensor σ over the surface. Therefore the forces and torques acting on the particle are

$$\begin{aligned} \boldsymbol{F} &= \int_S \sigma \cdot \mathrm{d}\boldsymbol{S} , \\ \boldsymbol{T} &= \int_S (\boldsymbol{x} - \boldsymbol{y}) \times \sigma \cdot \mathrm{d}\boldsymbol{S} . \end{aligned} \tag{3.9}$$

To complete the problem formulation, the particle trajectory is governed by Newton's equations

$$m\ddot{\boldsymbol{y}} = \boldsymbol{F} , \quad \frac{\mathrm{d}}{\mathrm{d}t}(\mathbb{I}\boldsymbol{\omega}) = \boldsymbol{T} . \tag{3.10}$$

Here dots denote the time derivative, m is the particle mass, and $\mathbb{I}$ its moment-of-inertia tensor.

The coupled equations (3.7-3.10) describe the motion of both particle and fluid. However, they are incredibly complicated because of their non-linearities: the so-called *convective term* $(\boldsymbol{u} \cdot \nabla)\boldsymbol{u}$ in Eq. (3.7), and the coupling through the moving boundary conditions (3.8).

We may understand that the problem is very hard just by imagining a particle in a fluid: as the particle moves and rotates, it stirs up a wake and vortices in its trail. These disturbances may linger and affect the particle at a later time. It seems that we are, in general, obliged to take into account the whole joint history of the particle and the fluid to predict the final state of the two. These complications raise the need for approximation, and *effective equations* for the particle motion.

3.2 Effective equations of motion

For the purposes of this thesis, the term *effective equations of motion* means a set of equations for the particle motion that does not involve the equations of fluid motion. The effective equations should be an approximation to the exact equations (3.7-3.10) in some limit.

In principle that means that the force on the particle is a functional of the particle trajectory and the background flow field $\boldsymbol{u}^\infty$:

$$\boldsymbol{F}_{\text{eff}} = \boldsymbol{g}(\boldsymbol{y}, \mathbb{R}, \boldsymbol{u}^\infty). \tag{3.11}$$

A concrete and well-known example is the Stokes force on a spherical particle of radius a

$$\boldsymbol{F}_{\text{Stokes}} = 6\pi\mu a(\boldsymbol{u}^\infty(\boldsymbol{y}, t) - \dot{\boldsymbol{y}}), \tag{3.12}$$

which we will discuss in detail shortly. Another example is the Stokes-Boussinesq force on a sphere accelerating in a still fluid:

$$\boldsymbol{F}_{\text{SB}} = -6\pi\mu a\dot{\boldsymbol{y}} - \frac{m}{2}\frac{\rho_f}{\rho_p}\ddot{\boldsymbol{y}} - 6a^2\sqrt{\pi\rho_f\mu}\int_0^t \frac{\ddot{\boldsymbol{y}}(\tau)\mathrm{d}\tau}{\sqrt{t-\tau}}. \tag{3.13}$$

This force depends on the history of the particle acceleration, and it is appropriate to describe rapidly accelerating particles. It is for example necessary to use Eq. (3.13) to describe the velocity of a particle in thermally agitated Brownian motion [18, 19].

The use of an effective equation is also called a *one-way coupling* approximation, because it explicitly gives the effect of the fluid on the particle, but not the other way around. We can therefore first compute, or choose, a flow

field $\boldsymbol{u}^\infty$ in absence of any particles, and then use the effective equation to calculate the particle motion. This is a great simplification over solving the exact coupled system. It is a very common method to study for example the motion of particles in turbulence (for example, in Paper F).

But we have to be careful. In the derivation of the Stokes force, for example, it is assumed that the particle is alone in the fluid. If we use the Stokes force to consider several particles simultaneously and they happen to move close to each other, the approximation is no longer valid. In that case, we must create an effective equation for the particle pair instead. If the particle moves close to a wall, we have to make yet another equation for that. The price of simplicity is specialization.

3.2.1 The particle Reynolds number

My specialization is the the effective equations valid for "small" particles. The Stokes force in Eq. (3.12) was derived in 1851 [13] and is the first example of this specialization. Let me explain this limit more precisely.

As explained above, a particle moving through a fluid creates disturbances that may come back and affect the particle at a later time. We are aiming for the limit where the disturbances will be smeared out by the viscosity before they make any secondary impact. This happens if the time for viscosity to smoothen the flow field is much smaller than the time it takes for the flow field to transport the disturbance over the particle size. The condition is precisely that the dimensionless particle Reynolds number is small. As stated in Sec. 2.1,

$$\mathrm{Re_p} = \frac{\text{Viscous time}}{\text{Time for fluid to flow one particle length}}. \tag{3.14}$$

More specifically,

$$\mathrm{Re_p} = \frac{a^2/\nu}{a/u_0} = \frac{u_0 a}{\nu}. \tag{3.15}$$

Here u_0 is a typical flow speed relative to the particle surface, a is the size of the particle and ν is the kinematic viscosity of the fluid. We see that the limit I call "small particles" is actually that of either small particles, or large viscosity, or slow motions. The Reynolds number determines whether the inertia of the fluid is important compared to the viscosity.

In my work on rotating particles in shear flows, the typical flow speed is $u_0 = sa$, where s is the shear rate of units $^1/_{\text{time}}$ (the shear flow is explained in detail in Section 3.4.) The resulting dimensionless number is sometimes called the shear Reynolds number

$$\mathrm{Re}_s = \frac{sa^2}{\nu}. \tag{3.16}$$

We introduce the dimensionless numbers in our equations by changing all variables into dimensionless variables using the available dimensions of the problem: length a and time $1/s$. In my case the change of variables is $\boldsymbol{u} = sa\boldsymbol{u}'$, $p = \mu sp'$, $\boldsymbol{x} = a\boldsymbol{x}'$, and $t = t'/s$. We make this change in Eq. (3.7), drop the primes, and find

$$\mathrm{Re}_s\left(\frac{\partial}{\partial t}\boldsymbol{u} + (\boldsymbol{u}\cdot\nabla)\boldsymbol{u}\right) = \nabla\cdot\mathfrak{o}, \quad \nabla\cdot\boldsymbol{u} = 0, \quad \mathfrak{o} = -p\mathbb{1} + 2\mathbb{S}. \tag{3.17}$$

When $\mathrm{Re}_s \ll 1$ we can hope to compute the force and torque on a particle by perturbation theory. The Stokes approximation is to set $\mathrm{Re}_s = 0$, and solve $\nabla\cdot\mathfrak{o} = 0$. This important limit is the topic of Section 3.3.

Let me make a general remark about de-dimensionalisation and changes of variables. Mathematically, we assume nothing by just making a change of variables such as that from Eq. (3.7) to (3.17). If we solve Eq. (3.17) *exactly* and transform the result back to dimensionful variables, we find the exact solution to Eq. (3.7). However, if we solve Eq. (3.17) asymptotically as $\mathrm{Re}_s \to 0$, the change of variables determines the relative importance of the terms in Eq. (3.7), and therefore the resulting asymptotic solution. If we choose another change of variables, say $t = a^2t'/\nu$, Eq. (3.17) is modified. In this case we find instead

$$\frac{\partial}{\partial t}\boldsymbol{u} + \mathrm{Re}_s(\boldsymbol{u}\cdot\nabla)\boldsymbol{u} = \nabla\cdot\mathfrak{o}, \quad \nabla\cdot\boldsymbol{u} = 0, \quad \mathfrak{o} = -p\mathbb{1} + 2\mathbb{S}. \tag{3.18}$$

Again, if we solve Eq. (3.18) *exactly* and transform the result back to dimensionful variables we find the exact solution to Eq. (3.7). But the asymptotic solution of Eq. (3.18) as $\mathrm{Re}_s \to 0$ is qualitatively different from that of Eq. (3.17). The choice of dimensionless variables embodies the physical assumptions that are effected by the perturbation theory. For the force on a translating sphere, this change in time scaling is responsible for the difference between the Stokes and the Stokes-Boussinesq forces in Eqs. (3.12) and (3.13).

3.2.2 The Stokes number

If we change the variables in the fluid equations, we must also make the corresponding changes in the coupled particle equations. The equation for the angular dynamics, for instance, becomes[1]

$$\mathrm{St}\frac{\mathrm{d}}{\mathrm{d}t}(\mathbb{I}\boldsymbol{\omega}) = \boldsymbol{T}\,, \quad \mathrm{St} = \frac{\rho_p}{\rho_f}\mathrm{Re}_s\,. \tag{3.19}$$

Another dimensionless number shows up: the Stokes number St. The Stokes number determines whether the particle inertia is important compared to the fluid forces. It is therefore not surprising that the Stokes number is related to the particle Reynolds number. They both compare inertial effects to the viscous forces. The only difference is through their relative densities. If the particle is heavier, its inertia is more important than the inertia of the fluid, and vice versa.

A neutrally buoyant particle has the same density as the fluid: $\rho_p = \rho_f$, and $\mathrm{St} = \mathrm{Re}_s$. This means that when we assume Re_s small, we also assume St small. If the densities are different, the particle will sink or float and we must consider its translation, unless $\mathrm{Re}_s = \mathrm{St} = 0$. In this thesis I consider only the orientation of the particle, and consequently I take $\mathrm{St} = \mathrm{Re}_s$.

3.3 The Stokes approximation

In the case when $\mathrm{Re}_s = 0$, the Navier-Stokes equation (3.17) reduces to the linear Stokes equation $\nabla \cdot \boldsymbol{\sigma} = 0$:

$$\nabla^2 \boldsymbol{u} = \nabla p\,, \quad \nabla \cdot \boldsymbol{u} = 0\,. \tag{3.20}$$

This type of flow is called viscous flow, or creeping flow. Such flows are completely dominated by viscosity, and disturbances are assumed to disappear so quickly that they do not even exist in the equations: there is no time derivative in Eq. (3.20). Stokes equations are linear, and therefore many problems admit analytical solution. In particular, the force and torque on a particle in linear viscous flow has been worked out in quite some detail [16, 17, 20, 21].

[1] I am sweeping some finer details under the carpet here. They are irrelevant for this argument, and you'll find it all in Sec. III in Paper C.

The fundamental result is that the force and torque on a small particle suspended in a flow is linearly related to the undisturbed flow. Given the particle velocity $\dot{\boldsymbol{y}}$ and angular velocity $\boldsymbol{\omega}$, we write the force $\boldsymbol{F}$ and torque $\boldsymbol{T}$ as

$$\begin{aligned}\boldsymbol{F} &= \mathscr{A}(\boldsymbol{u}-\dot{\boldsymbol{y}})+\mathscr{B}(\boldsymbol{\Omega}-\boldsymbol{\omega})+\mathscr{G}:\mathbb{S},\\ \boldsymbol{T} &= \mathscr{B}^{\mathrm{T}}(\boldsymbol{u}-\dot{\boldsymbol{y}})+\mathscr{C}(\boldsymbol{\Omega}-\boldsymbol{\omega})+\mathscr{H}:\mathbb{S}.\end{aligned} \tag{3.21}$$

Here $\mathbb{S}$ and $\boldsymbol{\Omega}$ are the flow gradients as explained in Section 3.1.1. The resistance tensors $\mathscr{A}$, $\mathscr{B}$, $\mathscr{C}$, $\mathscr{G}$ and $\mathscr{H}$ depend only on the particle shape, and can be computed once and for all [16]. The tensors $\mathscr{G}$ and $\mathscr{H}$ are of rank three, and the double dot product $\mathscr{H}:\mathbb{S}$ is a contraction over two indices. In index notation it reads $(\mathscr{H}:\mathbb{S})_i = H_{ijk}S_{jk}$ (with implied summation over repeated indices).

The resistance tensors in the case of a sphere of radius a are $\mathscr{A} = 6\pi\mu a\mathbb{1}$, $\mathscr{B} = \mathscr{G} = \mathscr{H} = 0$ and $\mathscr{C} = 8\pi\mu a^3\mathbb{1}$. In fact, for any particle that is mirror-symmetric in three orthogonal planes it holds that $\mathscr{B} = 0$ [20]. In such cases there is neither coupling between rotation and force, nor between translation and torque. An example of the contrary is a cork-screw-shaped particle. However, this thesis concerns particles with shapes such that the orientational dynamics decouple from the translational motion.

There is a hidden complication in Eq. (3.21): the flow is usually known in a fixed frame of reference, but the resistance tensors are known in the frame of reference of the particle. Expressing the resistance tensors in the fixed frame of reference entails a rotation dependent on the particle orientation. Thus, the torque is in general a non-linear function of particle orientation.

The Stokes resistance of a rotating ellipsoid was computed in a now famous paper by Jeffery in 1922 [2]. The result therein is of course not expressed in the subsequently invented tensor notation, but all the necessary calculations are there. The adaptation to current notation is found in *Microhydrodynamics* (Ref. 16 p. 56). Jeffery's result is the basis of all my work, so I dedicate Section 3.5 to discuss it in detail, but first we must discuss the anatomy of the simple shear flow in Section 3.4.

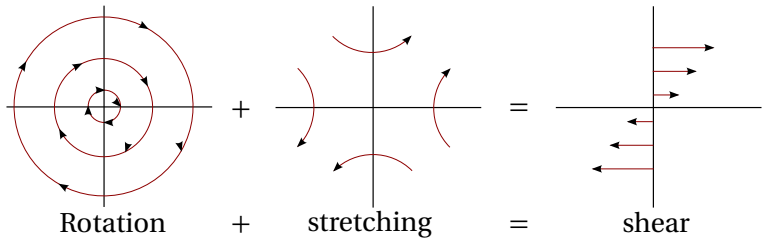

Figure 3.1: Decomposition of the simple shear flow into rotation and strain.

3.4 Simple shear flow

The simple shear flow is a uni-directional linear flow which varies in magnitude in only one transversal direction. It is shown in Fig. 3.1. The equation describing the shear flow is simply,

$$\boldsymbol{u}(y) = s\, y\, \hat{\boldsymbol{x}}. \tag{3.22}$$

Here s is a scalar called the shear strength, and y is the coordinate along the $\hat{\boldsymbol{y}}$-axis. Fig. 3.2 shows the coordinate system we use for shear flows in this thesis and in the appended papers. The three principal directions are the flow direction $\hat{\boldsymbol{x}}$, the shear direction $\hat{\boldsymbol{y}}$ and the vorticity direction $\hat{\boldsymbol{z}}$. The vorticity direction $\hat{\boldsymbol{z}}$ is also the direction of $\boldsymbol{\Omega}$ introduced in Sec. 3.1.1.

The flow gradient of the simple shear flow is constant and in cartesian coordinates given by

$$\mathbb{A} = \begin{bmatrix} 0 & s & 0 \\ 0 & 0 & 0 \\ 0 & 0 & 0 \end{bmatrix}. \tag{3.23}$$

The shear flow is important for two reasons. First, it is one of the fundamental flows in rheology, the study of fluids. It is the flow inside an ideal Couette device, used for example to measure viscosity. Second, as far as particle dynamics go, the simple shear flow is relevant for *any* flow with parallel streamlines. Consider for example the laminar flow of a suspension through a pipe. The pipe is assumed to be large compared to the suspended particles, and the flow profile is most likely a complicated function of position y in the

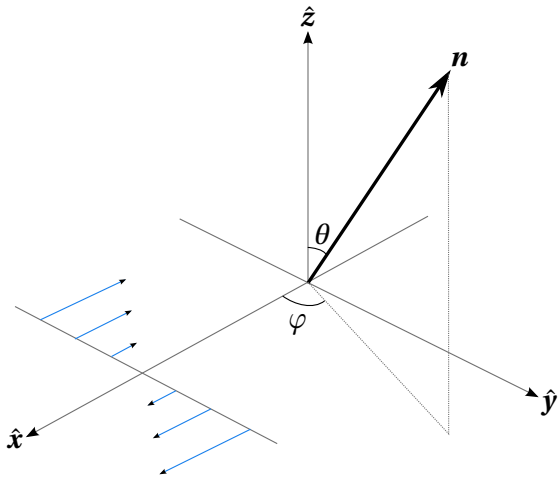

Figure 3.2: Coordinate system of simple shear flow in this thesis. The directions are the flow direction $\hat{\boldsymbol{x}}$, the shear direction $\hat{\boldsymbol{y}}$, and the vorticity direction $\hat{\boldsymbol{z}}$. The angles (θ, φ) are the spherical coordinates of the particle direction $\boldsymbol{n}$.

pipe cross section[2]:

$$\boldsymbol{u}(y) = f(y)\hat{\boldsymbol{x}}, \tag{3.24}$$

and the flow gradient is

$$\mathbb{A} = \begin{bmatrix} 0 & f'(y) & 0 \\ 0 & 0 & 0 \\ 0 & 0 & 0 \end{bmatrix}. \tag{3.25}$$

Thus, if the flow profile f varies slowly over the particle size, the particle experiences a simple shear flow of strength $f'(y)$. This is the case in the experiment described in Paper E.

Curiously, the dynamics of an ellipsoidal particle in a viscous shear flow offers a rich variety of behaviours. There is no stationary state, but a particle tumbles end-to-end indefinitely. If the particle is axisymmetric, the tumbling is periodic. The technical details and explanations of this are discussed in

[2] In principle the function should also depend on the position in the z-direction. In that case the result is also a simple shear flow, although rotated.

Sec. 3.5, but we can understand the underlying reason from the composition of the shear flow. Fig. 3.1 illustrates schematically how the shear is a superposition of two flows. One is a pure rotation, corresponding to the antisymmetric part $\mathbb{O}$ of the flow gradient. The other is a pure strain, the symmetric part $\mathbb{S}$ of the flow gradient. Now imagine a rod-shaped particle in these flows. The pure rotation, the vorticity, will rotate the rod with a constant angular velocity, regardless of the rod's orientation. The strain, on the other hand, has a preferred direction to which it will attract the long axis of the rod. Sometimes the vorticity and strain will cooperate to turn the rod onto the strain eigendirection, and sometimes the vorticity will struggle to rotate the rod out of the attracting direction. The result is that the rod will always rotate, but sometimes faster and sometimes slower. When the difference between the fast and the slow rotations is large, we perceive this as intermittent tumbling.

3.5 The Jeffery equation and its solutions

The main result of Jeffery [2] is the hydrodynamic torque $\boldsymbol{T}$ on a general ellipsoid rotating in a viscous shear flow (his Eq. (36)). In other words, he computed the elements of the resistance tensors in Eq. (3.21). Some elements were known to Jeffery from earlier work by Oberbeck [22] and Edwardes [23]. However, Jeffery completed what is arguably the hardest part of the calculation, and has received the most credit for this work.

The viscous torque is calculated neglecting the effects of fluid inertia, $\mathrm{Re}_s = 0$. To be consistent (see Section 3.2.2) we also neglect the effects of particle inertia, $\mathrm{St} = 0$. This is the overdamped limit where the equation of motion is determined by a static force and torque balance. Jeffery [2] found the angular velocity of the particle by solving $\boldsymbol{T} = 0$. Here I give the result in my notation, the details are available in Appendix A.

We represent the shape and orientation of an ellipsoid by the lengths (a_1, a_2, a_3) and directions $(\boldsymbol{n}_1, \boldsymbol{n}_2, \boldsymbol{n}_3)$ of the three half-axes. Then $\boldsymbol{n}_1$ gives the direction of the axis with length a_1, and so on. The angular velocity of the particle depends on the flow gradients, the particle orientation and the aspect ratios of the particle as

$$\boldsymbol{\omega} = \boldsymbol{\Omega} + \frac{\Lambda - K}{K\Lambda - 1}\left(\boldsymbol{n}_2^{\mathrm{T}}\mathbb{S}\boldsymbol{n}_3\right)\boldsymbol{n}_1 + \Lambda\left(\boldsymbol{n}_3^{\mathrm{T}}\mathbb{S}\boldsymbol{n}_1\right)\boldsymbol{n}_2 - K\left(\boldsymbol{n}_1^{\mathrm{T}}\mathbb{S}\boldsymbol{n}_2\right)\boldsymbol{n}_3\,, \tag{3.26}$$

where

$$K = \frac{\kappa^2 - 1}{\kappa^2 + 1}, \qquad \Lambda = \frac{\lambda^2 - 1}{\lambda^2 + 1}, \qquad \lambda = a_3/a_1, \qquad \kappa = a_2/a_1\,. \tag{3.27}$$

Here $\boldsymbol{\Omega}$ and $\mathbb{S}$ are the flow rotation and strain as defined in Section 3.1.1. The coefficients Λ and K are the *shape parameters*, and for an ellipsoid $-1 < \Lambda, K < 1$. A sphere is described by $\Lambda = K = 0$. If either Λ or K is zero, the particle is an axisymmetric spheroid. Eq. (3.26) is valid for most particles with the same mirror symmetries as an ellipsoid, with a suitable redefinition of Λ and K [16, 17, 24]. More precisely, there are other particle shapes described by resistance tensors of the same *form*, but different numerical values of the elements.

We rename $\boldsymbol{n} = \boldsymbol{n}_3$ and $\boldsymbol{p} = \boldsymbol{n}_2$, and compute their equation of motion by $\dot{\boldsymbol{n}}_i = \boldsymbol{\omega} \times \boldsymbol{n}_i$ (details in Appendix A):

$$\begin{aligned}
\dot{\boldsymbol{n}} &= \mathbb{O}\boldsymbol{n} + \Lambda\big(\mathbb{S}\boldsymbol{n} - (\boldsymbol{n}^{\mathrm{T}}\mathbb{S}\boldsymbol{n})\boldsymbol{n}\big) + \frac{K(1-\Lambda^2)}{K\Lambda - 1}\big(\boldsymbol{n}^{\mathrm{T}}\mathbb{S}\boldsymbol{p}\big)\boldsymbol{p}, \\
\dot{\boldsymbol{p}} &= \mathbb{O}\boldsymbol{p} + K\big(\mathbb{S}\boldsymbol{p} - (\boldsymbol{p}^{\mathrm{T}}\mathbb{S}\boldsymbol{p})\boldsymbol{p}\big) + \frac{\Lambda(1-K^2)}{K\Lambda - 1}\big(\boldsymbol{n}^{\mathrm{T}}\mathbb{S}\boldsymbol{p}\big)\boldsymbol{n}\,.
\end{aligned} \tag{3.28}$$

Eq. (3.28) is the Jeffery equation of motion for a the axes of an triaxial ellipsoid. Recall that $\mathbb{O}\boldsymbol{n} = \boldsymbol{\Omega} \times \boldsymbol{n}$. The motion of the third axis is fully determined by $\boldsymbol{n}_3 = \boldsymbol{n} \times \boldsymbol{p}$. The equations are symmetric under the simultaneous exchange of $\Lambda \longleftrightarrow K$ and $\boldsymbol{n} \longleftrightarrow \boldsymbol{p}$, because the new equations describe the same physical situation with the axes permuted.

For a simple shear flow Eq. (3.28) is *reversible* in the general sense [25]: the equations are symmetric under $(t, n_x, p_x) \to (-t, -n_x, -p_x)$, with $\hat{\boldsymbol{x}}$ the flow direction of the shear flow. A reversible dynamical system shares many properties with conservative ('Hamiltonian') systems [25]. In particular, around any elliptic fixed point there must exist a family of periodic orbits. In Section 3.5.2 we will see that this is exactly the case for the solutions of Eq. (3.28) for a triaxial particle in shear flow.

In the following we will study the solutions to Eq. (3.28) in some detail. But it is helpful to first inspect the meaning of the different terms in the equation of motion:

The first term means that the particle is rotated by the local flow vorticity, and that this rotation is independent of the particle shape.

The second term means that the local rate-of-strain attracts the particle axis to the strongest eigendirection of $\mathbb{S}$. The strength of the attraction is affected by the particle shape. The more elongated an axis is, the stronger the attraction becomes. The non-linear part $-(\boldsymbol{n}^{\mathrm{T}}\mathbb{S}\boldsymbol{n})\boldsymbol{n}$ simply preserves the unit magnitude of the vector $\boldsymbol{n}$, and it has no physical meaning. This fact is explained in detail in Section 3.5.1.

The third and last term couples the motion of $\boldsymbol{n}$ and $\boldsymbol{p}$. This is because the local rate-of-strain will try to align all elongated axes. But since the particle is a rigid body, this is not possible. Instead there is competition, and the outcome depends on the relative elongation of the axes. If the particle is axisymmetric, say $K = 0$, there is only one elongated axis and therefore no competition. This case is described in detail in Section 3.5.1. The general case of a triaxial ellipsoid in a simple shear flow is discussed in Section 3.5.2.

3.5.1 Axisymmetric particles

In this section we consider axisymmetric particles: particles which are rotationally symmetric around an axis of symmetry. For such particles the shape factor $K = 0$, and Eq. (3.28) reduces to

$$\dot{\boldsymbol{n}} = \mathbb{O}\boldsymbol{n} + \Lambda\big(\mathbb{S}\boldsymbol{n} - (\boldsymbol{n}^{\mathrm{T}}\mathbb{S}\boldsymbol{n})\boldsymbol{n}\big), \tag{3.29}$$

$$\dot{\boldsymbol{p}} = \mathbb{O}\boldsymbol{p} - \Lambda\big(\boldsymbol{n}^{\mathrm{T}}\mathbb{S}\boldsymbol{p}\big)\boldsymbol{n}\,. \tag{3.30}$$

The vector $\boldsymbol{n}$ describes the direction of the symmetry axis of the particle, see Fig. 3.3. The vector $\boldsymbol{p}$ describes the rotation around the symmetry axis. The equations for $\boldsymbol{n}$ and $\boldsymbol{p}$ are decoupled: we may first solve Eq. (3.29) for $\boldsymbol{n}(t)$, then Eq. (3.30) is a linear equation for $\boldsymbol{p}(t)$. In this Section we will neglect the dynamics of $\boldsymbol{p}$, it is discussed in Section 3.5.2.

Eq. (3.29) is a non-linear vector equation, and as such it is seemingly hard to solve. However, the non-linearity is only apparent: it is due to the geometric constraint that $\boldsymbol{n}$ is a unit vector. The underlying dynamics is in fact linear. I will now explain two ways to understand this fact.

The vorticity $\mathbb{O}$ rotates $\boldsymbol{n}$, and the strain $\mathbb{S}$ aligns and stretches $\boldsymbol{n}$ towards its strongest eigendirection. The non-linear term $\boldsymbol{n}\boldsymbol{n}^{\mathrm{T}}\mathbb{S}\boldsymbol{n}$ is simply the stretching component of the strain, which is subtracted in order to prevent elongation of $\boldsymbol{n}$. Bretherton (Sec. 6 in Ref. 24) realised that we may instead model the orientation of the particle with any vector $\boldsymbol{q}$ which obeys the same

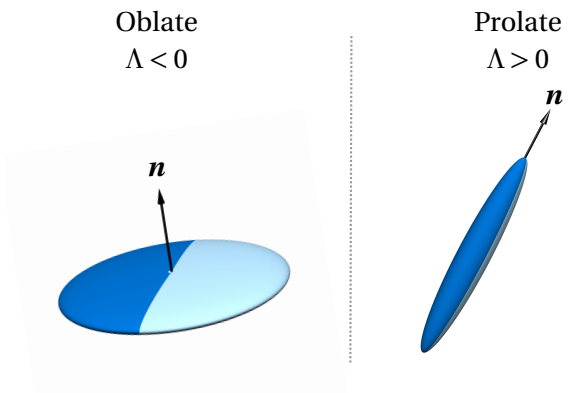

Figure 3.3: Illustration of axisymmetric particles and the definition of the vector $\boldsymbol{n}$. *Left*: Oblate, disk-shaped particle. *Right*: Prolate, rod-shaped particle.

linear terms, but without compensating for any elongation:

$$\dot{\boldsymbol{q}} = (\mathbb{O} + \Lambda\mathbb{S})\boldsymbol{q}. \tag{3.31}$$

Owing to the common linear terms in Eq. (3.29) and Eq. (3.31), the vector $\boldsymbol{q}$ will have the same angular dynamics as $\boldsymbol{n}$. In addition, $\boldsymbol{q}$ may be stretched and compressed by the strain $\mathbb{S}$. But since we are only interested in the angular degrees of freedom, we can at any instant recover $\boldsymbol{n}$ by normalising $\boldsymbol{q}$ to unit length. Thus, the general solution of the Jeffery equation is given by solving Eq. (3.31) for $\boldsymbol{q}(t)$, then the solution to Eq. (3.29) is given by normalising $\boldsymbol{q}(t)$ to unit length:

$$\boldsymbol{n}(t) = \frac{\boldsymbol{q}(t)}{|\boldsymbol{q}(t)|}. \tag{3.32}$$

Another, more mathematical, way of understanding how the linear companion equation (3.31) arises is the following. Like above, we choose to represent the particle orientation by a vector $\boldsymbol{q}$ which is parallel to $\boldsymbol{n}$. Define $\boldsymbol{q} = \alpha(t)\boldsymbol{n}$, with $\alpha(t)$ an arbitrary function of time. We know from this definition that we may always recover $\boldsymbol{n}$ by normalising $\boldsymbol{q}$ to unit length. Now, we can calculate the equation of motion for $\boldsymbol{q}$:

$$\frac{\mathrm{d}\boldsymbol{q}}{\mathrm{d}t} = \frac{\mathrm{d}}{\mathrm{d}t}(\alpha\boldsymbol{n}) = \dot{\alpha}\boldsymbol{n} + \alpha\left(\mathbb{O}\boldsymbol{n} + \Lambda\left(\mathbb{S}\boldsymbol{n} - \boldsymbol{n}\boldsymbol{n}^{\mathrm{T}}\mathbb{S}\boldsymbol{n}\right)\right). \tag{3.33}$$

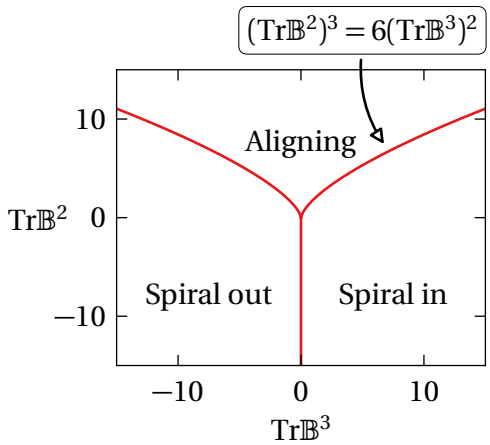

Figure 3.4: Map of the three possible types of particle motion, as determined by the eigensystem of $\mathbb{B} = \mathbb{O} + \Lambda\mathbb{S}$. On the red line between "Spiral out" and "Spiral in" the motion is on a closed orbit.

But $\alpha(t)$ is an arbitrary function which we may choose. In particular we can choose $\alpha(t)$ to be a function satisfying

$$\dot{\alpha} = \alpha\Lambda \boldsymbol{n}^{\mathrm{T}}\mathbb{S}\boldsymbol{n}. \tag{3.34}$$

By inserting this choice of $\alpha(t)$ into Eq. (3.33), we again arrive at Eq. (3.31).

We now consider the solutions of Jeffery's equation in a time-independent linear flow. This case includes for example the simple shear flow. It is also a useful model when the flow changes only slowly in time, compared to the time it takes for the gradients to affect the particle orientation. First, I will describe the possible solutions of Eq. (3.29) in linear flows. Second, I will discuss the solutions of Jeffery's equation in a simple shear flow. These solutions are called the Jeffery orbits, and they play an important role in Papers A-E.

When $\mathbb{O}$ and $\mathbb{S}$ are time-independent the linear companion equation (3.31) is solved by the matrix exponential:

$$\boldsymbol{q}(t) = e^{(\mathbb{O}+\Lambda\mathbb{S})t}\boldsymbol{q}(0). \tag{3.35}$$

This solution implies that the long-time dynamics of $\boldsymbol{q}$, and therefore $\boldsymbol{n}$, is determined by the eigenvalues and eigenvectors of the matrix $\mathbb{B} = \mathbb{O} + \Lambda\mathbb{S}$. For an incompressible flow $\mathrm{Tr}\mathbb{B} = 0$, because $\mathrm{Tr}\mathbb{A} = 0$. In three spatial dimensions, the three eigenvalues of $\mathbb{B}$ must sum to zero. Thus, as noted by Bretherton [24], there are four distinct possibilities for the eigensystem of $\mathbb{B}$:

1. Three real eigenvalues, then

   $\boldsymbol{q}$ aligns with the eigenvector corresponding to the largest eigenvalue.

2. One real eigenvalue $a > 0$, and a complex pair $-a/2 \pm i\omega$, then

   $\boldsymbol{q}$ spirals into alignment with the eigenvector corresponding to the real eigenvalue.

3. One real eigenvalue $a < 0$, and a complex pair $-a/2 \pm i\omega$, then

   $\boldsymbol{q}$ spirals out towards infinity in the plane that contains the origin and is spanned by the real and imaginary parts of the complex eigenvector.

4. One real eigenvalue $a = 0$, and an imaginary pair $\pm i\omega$, then

   $\boldsymbol{q}$ rotates indefinitely in a closed elliptic orbit in a plane that contains the initial condition and is spanned by the real and imaginary parts of the complex eigenvector.

The characteristic equation for the eigenvalues b of a 3×3-matrix $\mathbb{B}$ is

$$-b^3 + b^2 \mathrm{Tr}\mathbb{B} + \frac{b}{2}\left(\mathrm{Tr}\mathbb{B}^2 - (\mathrm{Tr}\mathbb{B})^2\right) + \det\mathbb{B} = 0. \tag{3.36}$$

But for a traceless matrix $\mathrm{Tr}\mathbb{B} = 0$ and $\det\mathbb{B} = \mathrm{Tr}\mathbb{B}^3/3$, because

$$\mathrm{Tr}\mathbb{B} = b_1 + b_2 + b_3 = 0 \implies b_3 = -(b_1 + b_2), \tag{3.37}$$

therefore

$$\mathrm{Tr}\mathbb{B}^3 = b_1^3 + b_2^3 + b_3^3 = -3(b_1^2 b_2 + b_1 b_2^2), \tag{3.38}$$

$$\det\mathbb{B} = b_1 b_2 b_3 = -(b_1^2 b_2 + b_1 b_2^2). \tag{3.39}$$

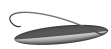

Thus the characteristic equation simplifies to

$$-b^3 + \frac{b}{2}\mathrm{Tr}\mathbb{B}^2 + \frac{1}{3}\mathrm{Tr}\mathbb{B}^3 = 0. \tag{3.40}$$

It is possible to solve Eq. (3.40) exactly for the eigenvalues, but the important observation is that they are determined by only two parameters: $\mathrm{Tr}\mathbb{B}^2$ and $\mathrm{Tr}\mathbb{B}^3$. In Fig. 3.4 I illustrate how the three cases outlined above correspond to different values of $\mathrm{Tr}\mathbb{B}^2$ and $\mathrm{Tr}\mathbb{B}^3$. The boundary curve of the region of three real eigenvalues is where the discriminant Δ of the characteristic equation is zero:

$$\Delta = \left(\mathrm{Tr}\mathbb{B}^2\right)^3 - 6\left(\mathrm{Tr}\mathbb{B}^3\right)^2 = 0. \tag{3.41}$$

In the region where there is a pair of complex eigenvalues, the two cases of spiral in or out are separated by $\mathrm{Tr}\mathbb{B}^3 = 0$. For any given flow gradient, changing the particle from rod-like to disk-shaped (or vice versa) transforms $\mathrm{Tr}\mathbb{B}^3 \to -\mathrm{Tr}\mathbb{B}^3$ and therefore change the qualitative dynamics from aligning to rotating (or vice versa). This transformation may be understood because

$$\mathrm{Tr}\mathbb{B}^3 = 3\Lambda\mathrm{Tr}\mathbb{OOS} + \Lambda^3\mathrm{Tr}\mathbb{SSS}. \tag{3.42}$$

The other combinations of $\mathbb{S}$ and $\mathbb{O}$ which could be expected to contribute, such as $\mathrm{Tr}\mathbb{OOO}$, vanish identically because of symmetries of $\mathbb{O}$ and $\mathbb{S}$. As explained above, changing a particle from rod-like to disk-shaped implies a change of sign of the shape factor Λ. We discussed the implications of this observation for the tumbling of particles in turbulent and random flows in an earlier paper [26].

Jeffery Orbits

The remainder of this section concerns the case of simple shear flow. This case is characterised by $\mathrm{Tr}\mathbb{B}^3 = 0$ and $\mathrm{Tr}\mathbb{B}^2 < 0$. The simple shear has a special position among flows, and we understand the significance of the condition $\mathrm{Tr}\mathbb{B}^3 = 0$ from the above discussion: First, a change of particle shape does not change the qualitative dynamics. Both disk-shaped particles and rod-like particles rotate in a shear flow. Second, $\mathbb{B}$ has a zero eigenvalue, as seen from the characteristic equation (3.40). The zero eigenvalue is important, because it implies that the particle dynamics never forgets its initial condition.

The eigenvector of the zero eigenvalue is the vorticity direction[3], thus the component of $\boldsymbol{q}$ in the vorticity direction is constant in a shear flow. The other two eigenvalues form an imaginary pair, resulting in a periodic rotation of $\boldsymbol{q}$.

In summary, the dynamics of $\boldsymbol{q}$ in a simple shear flow is a periodic rotation in a plane. The plane is normal to the vorticity direction, and determined by the initial condition of $\boldsymbol{q}$.

When the trajectories $\boldsymbol{q}(t)$ are projected onto the unit sphere, the result $\boldsymbol{n}(t)$ are the Jeffery orbits. I visualise this in Fig. 3.5 where the trajectories $\boldsymbol{q}(t)$ and $\boldsymbol{n}(t)$ are shown for three different initial conditions.

The orbits on the north and south hemispheres are the same, because of the particle inversion symmetry: changing $\boldsymbol{n} \to -\boldsymbol{n}$ implies $\dot{\boldsymbol{n}} \to -\dot{\boldsymbol{n}}$. The orbits are also symmetric under a 180 degree rotation around the vorticity, $\boldsymbol{n} \to \mathbb{R}_\pi \boldsymbol{n}$ implies $\dot{\boldsymbol{n}} \to \mathbb{R}_\pi \dot{\boldsymbol{n}}$, becuse of the symmetry of the shear flow. These two symmetries together enforce that no orbit may cross the equator of the sphere, because on the equator the two symmetries coincide but have different sign. The Jeffery orbit which is exactly on the equator of the sphere is called the *tumbling orbit*, because the vector $\boldsymbol{n}$ tumbles in the flow-shear plane. The orbit at a pole of the sphere, where $\boldsymbol{n}$ is aligned with the vorticity direction, is called the *log-rolling* orbit. The name refers to the motion of a rod which rolls around its axis of symmetry, but the name is used for both prolate and oblate particles. Log-rolling for an oblate particle means that it spins like a frisbee. These particular orbits are depicted in Fig. 3.6.

The solutions to Jeffery's equation in a simple shear flow are degenerate: the orientational trajectory depends on the initial condition indefinitely. The degeneracy is a result of the assumptions made in the course deriving the Jeffery orbits. The Jeffery equation neglects the effects of both fluid and particle inertia. In fact, Jeffery suggested that inertia should dissolve the degeneracy and lead to a determinate prediction. My work in the Papers A-D resolves this question. Although Jeffery was right in principle, it did not turn out exactly like he envisaged it. This is described in detail in Section 4.

One might expect that the degeneracy of the Jeffery orbits is lifted for a particle that is not perfectly axisymmetric. This is not the case. However, the trajectories are much more intricate. This is the topic of Section 3.5.2.

[3] See Fig. 3.2 and Sec. 3.4 for the definition of the coordinate system and the terminology of its directions in a simple shear flow.

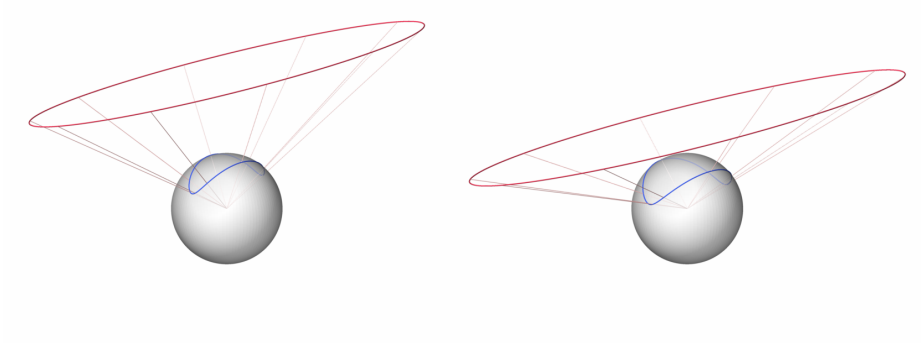

(a) **(b)**

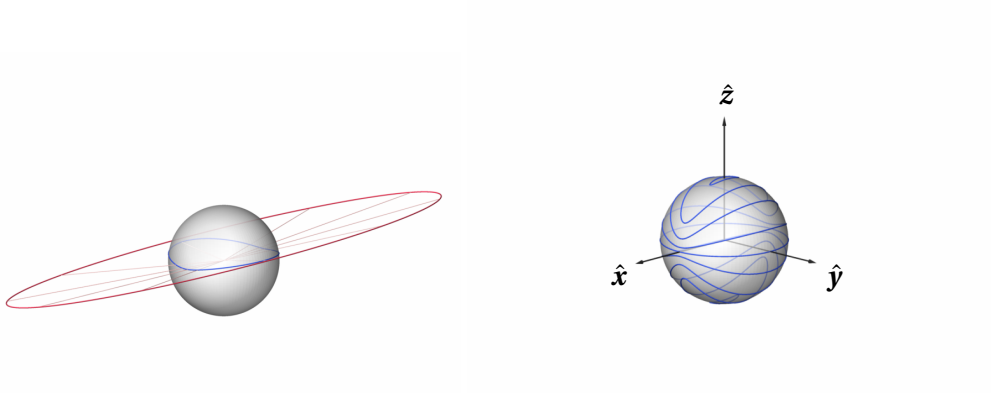

(c) **(d)**

Figure 3.5: (a-c) Illustrations of how the trajectories $\boldsymbol{q}(t)$ (red) produces the Jeffery orbits $\boldsymbol{n}(t)$ (blue) upon projection onto the unit sphere. **(d)** Sample of resulting Jeffery orbits with coordinate system. All trajectories correspond to a particle of aspect ratio $\lambda = 5$ in a simple shear flow.

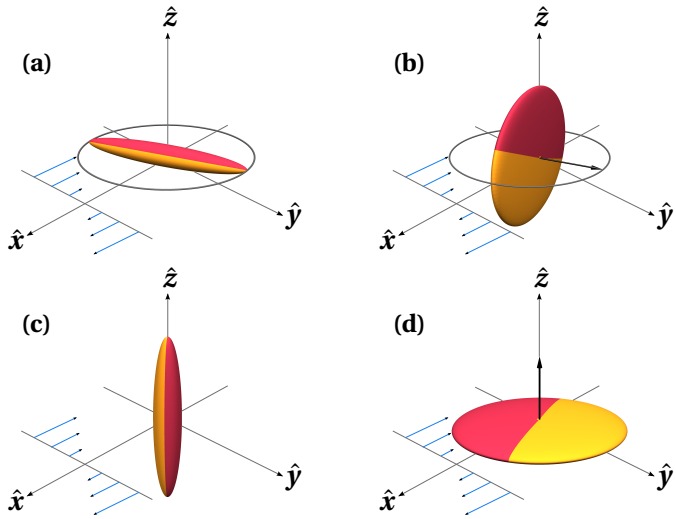

Figure 3.6: Illustration of the tumbling and log-rolling orbits it a simple shear flow. **(a)** prolate tumbling, **(b)** oblate tumbling, **(c)** prolate log-rolling, **(d)** oblate log-rolling.

3.5.2 Non-axisymmetric particles

In this Section I describe the solutions to the Jeffery equation (3.28) for a triaxial particle in a simple shear flow. It turns out that a triaxial particle also tumbles, but in a much more complicated fashion than the Jeffery orbits for an axisymmetric particle [27–29]. In general no closed form solutions are known, therefore we rely on numerical solutions in this section.

A rotation in three dimensions has three degrees of freedom, but in general it is complicated to represent rotations because there is no simple set of three coordinates which covers all rotations without singularities. The vectors $\boldsymbol{n}$ and $\boldsymbol{p}$ in Eq. (3.28) are physically intuitive, but mathematically their six components are strongly redundant because of the constraints $|\boldsymbol{n}| = |\boldsymbol{p}| = 1$ and $\boldsymbol{n} \cdot \boldsymbol{p} = 0$. For the purpose of visualisations, we use Euler angle coordinates in the Goldstein z-x'-z'' convention [30]: Start from $\boldsymbol{n}_i = \boldsymbol{e}_i$, with $\boldsymbol{e}_i$ a fixed frame of reference. First rotate the $\boldsymbol{n}_i$ by φ around $\boldsymbol{n}_3$, then by θ around the resulting $\boldsymbol{n}_1$ and finally by ψ around the resulting $\boldsymbol{n}_3$. With the shorthand

$c\,x = \cos x$ and $s\,x = \sin x$ the elements of the rotation matrix are

$$\mathbb{R} = \begin{pmatrix} c\varphi\, c\psi - c\theta\, s\varphi\, s\psi & c\psi\, s\varphi + c\theta\, c\varphi\, s\psi & s\theta\, s\psi \\ -c\theta\, c\psi\, s\varphi - c\varphi\, s\psi & c\theta\, c\varphi\, c\psi - s\varphi\, s\psi & c\psi\, s\theta \\ s\theta\, s\varphi & -c\varphi\, s\theta & c\theta \end{pmatrix}. \tag{3.43}$$

The rows of this matrix are the components of $\boldsymbol{n}_i$ along the coordinate axes $\boldsymbol{e}_i$. In particular the second and third rows are the elements of $\boldsymbol{p}$ and $\boldsymbol{n}$. Hinch & Leal [28] showed that in the absence of noise $\dot{\varphi} < 0$. This means that the tumbling of a triaxial particle shares one property with the Jeffery orbits: the vector $\boldsymbol{n}$ monotonically rotates around the vorticity. It is therefore natural to regard the orientation space as a torus, in which the deterministic trajectories go around, see Fig. 3.7. Each transversal slice of constant φ of this torus is a *Poincaré surface-of-section* [31] which intersects all trajectories, schematically shown in Fig. 3.7.

We follow Hinch & Leal [28] and choose the surface-of-section $\varphi = 2n\pi$. This corresponds to $n_x = 0, n_y < 0$. We solve Eq. (3.28) numerically for many different initial conditions. Every time a trajectory passes through the surface-of-section we plot a point at the corresponding value of $n_z = \cos\theta$ and ψ, see Fig. 3.8. Four examples for $\lambda = 5$ and increasing values of κ are shown in Figs. 3.9-3.12.

Fig. 3.9 shows the surface-of-section for an axisymmetric particle. The horizontal lines are the Jeffery orbits of an axisymmetric particle. Every time a trajectory reaches the surface-of-section, the value of n_z is the same, because the Jeffery orbits are strictly periodic in $\boldsymbol{n}$. However, it turns out that the value of ψ is in general not periodic. This means that the vector $\boldsymbol{p}$ does not, in general, make one revolution around $\boldsymbol{n}$ for every Jeffery orbit. The strict periodicity of the Jeffery orbits really only applies to the motion of the symmetry axis. This detail has no physical implications for the motion. But if we were to paint a pattern on a particle, and observe the motion experimentally, this aperiodicity would be apparent.

For the trajectory of a nearly axisymmetric particle neither n_z, nor ψ is constant. The structure of trajectories on the surface-of-section is more complicated, with closed ellipses near $n_z \approx 0$, and curved lines towards $n_z \approx \pm 1$, shown in Fig. 3.10. The point $(0,0)$ on the surface-of-section is an elliptic fixed point. As explained in Section 3.5 the dynamical system (3.28) is reversible, and consequently the dynamics around the fixed point is described by a one-parameter family of closed orbits [25].

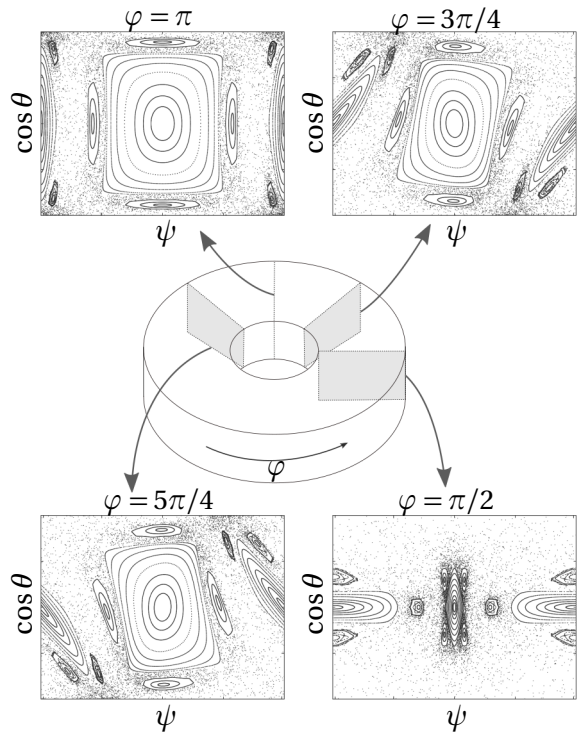

Figure 3.7: Schematic explanation of the surfaces-of-section for the orientational dynamics of triaxial ellipsoids in shear flow. The torus depicts the three-dimensional orientational space for an ellipsoid. The major axis of the ellipsoid rotates monotonously around the vorticity [28], depicted by the azimuthal angle φ along the torus. The surfaces-of-sections shown correspond to the major axis pointing the direction along the flow, along the extensional strain, perpendicular to the flow, and along the compressing strain. The surfaces-of-section at $\varphi \to \varphi+\pi$ are equal, because the flow is symmetric under this rotation. Surfaces-of-section computed by G. Almondo.

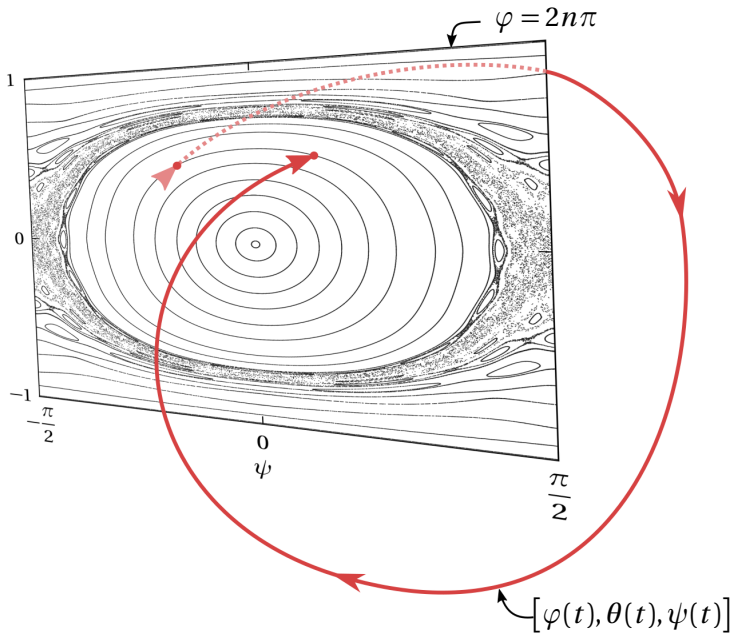

Figure 3.8: Illustration of the surface-of-section $\varphi = 2n\pi$. The trajectory (in red) starts at a point in the surface-of-section, makes one revolution of φ in phase-space, and returns to another point on the same curve in the surface-of-section. We create a picture of the surface-of-section by computing many trajectories with many different initial conditian and plotting a point at each hit.

A trajectory is always confined to the curve on which it started. In this sense the orientational dynamics of a triaxial particle is degenerate, just like the Jeffery orbits for an axisymmetric particle. No orbit is physically preferred over any other, but the dynamics are determined by the initial condition.

The degeneracy of these solutions may be broken by the effect of particle and fluid inertia, like in the case of axisymmetric particles. Lundell [32] show numerical simulations for $\mathrm{Re}_s = 0$ but $\mathrm{St} > 0$ which support this expectation. The method used in Papers A-D and Refs. [33, 34] can in principle be extended to the case of ellipsoids. However, that calculation will involve rather large amounts of algebra.

When we consider a significantly non-axisymmetric particle, the trajectories on the surface-of-section look very different, like in Fig. 3.11 and Fig. 3.12. Many initial conditions lead to deterministic chaos, which shows up as areas full of gray dots without apparent structure. A trajectory starting in this chaotic layer can go anywhere else inside it.

In Paper E we describe experimental observations of microsized glass rods in a microfluidic channel flow. We argue that their orientational motion is consistent with the solutions presented in this Section although the analysis is complicated by the fact that we can not resolve the angle ψ in the experiment. This is further described in Section 5 and Paper E.

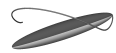

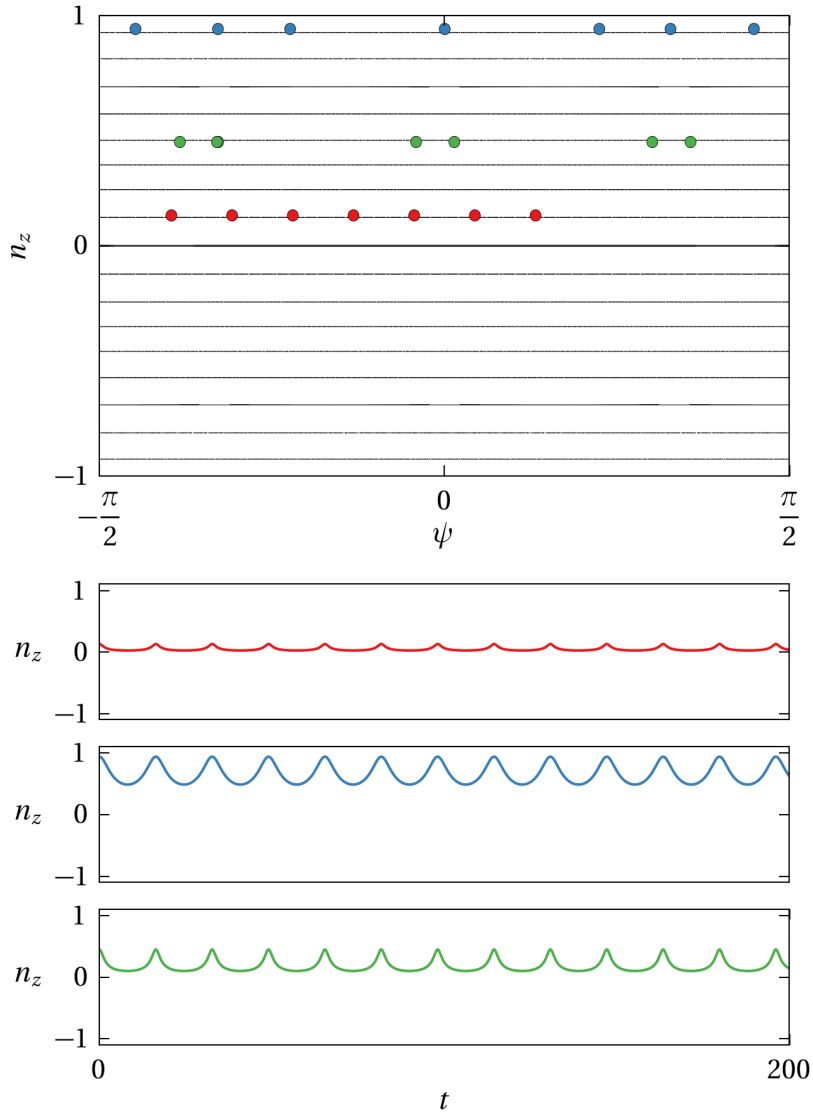

Figure 3.9: Top: Poincaré surface-of-section of an axisymmetric particle with aspect ratios $\lambda = 5$, $\kappa = 1$. Bottom: Examples of what $n_z(t)$ looks like, given the trajectory indicated by the color coded markers on the surface-of-section.

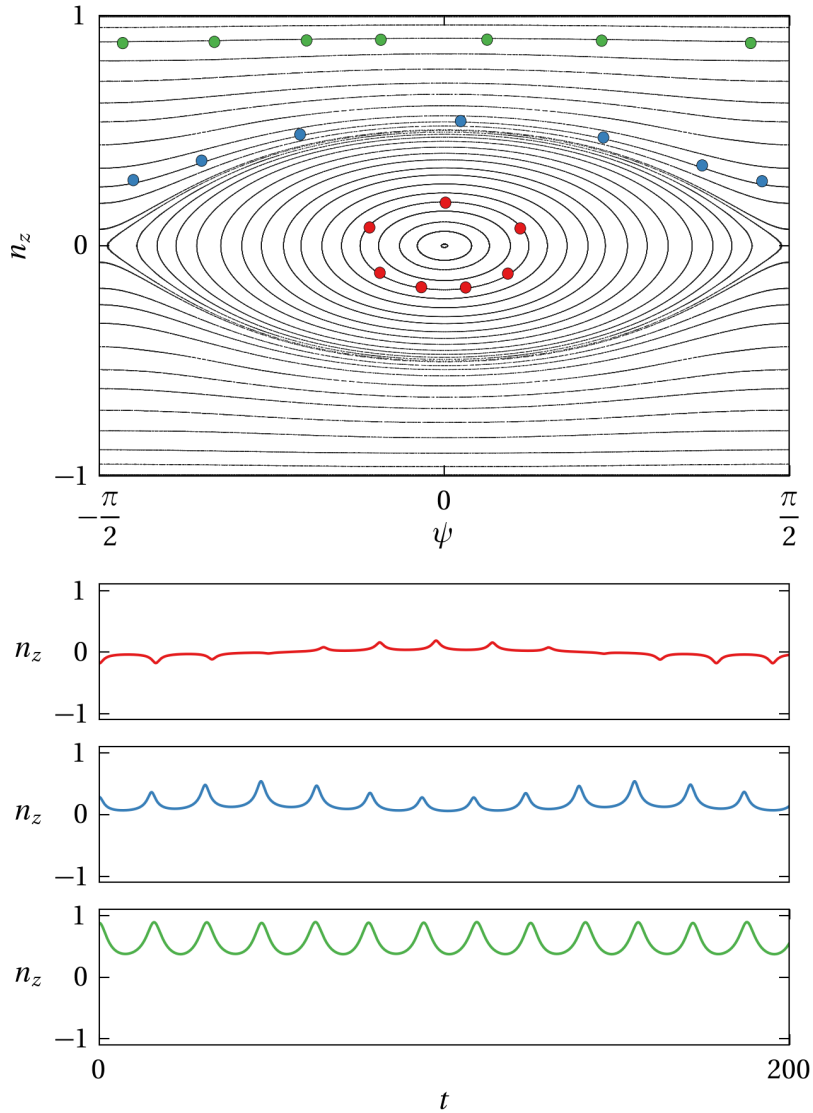

Figure 3.10: Top: Poincaré surface-of-section of an asymmetric particle with aspect ratios $\lambda = 5$, $\kappa = 1.1$. Bottom: Examples of what $n_z(t)$ looks like, given the trajectory indicated by the color coded markers on the surface-of-section.

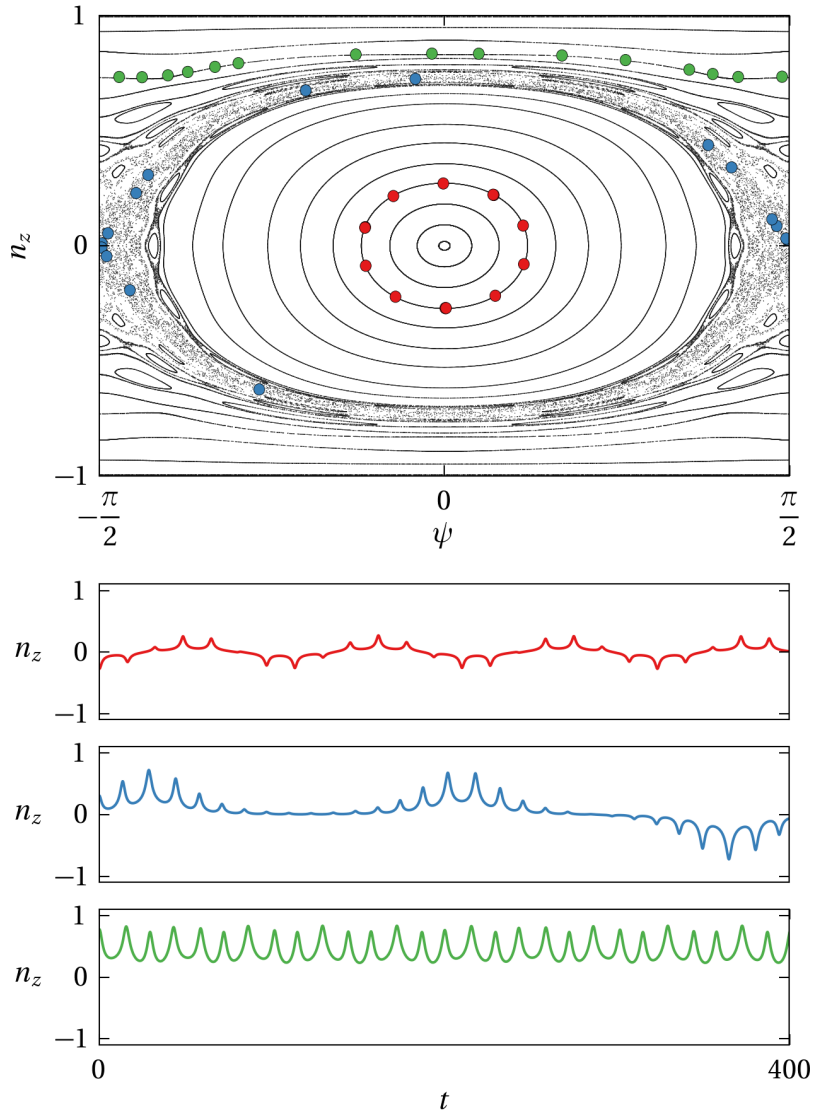

Figure 3.11: Top: Poincaré surface-of-section of an axisymmetric particle with aspect ratios $\lambda = 5$, $\kappa = 1.3$. Bottom: Examples of what $n_z(t)$ looks like, given the trajectory indicated by the color coded markers on the surface-of-section.

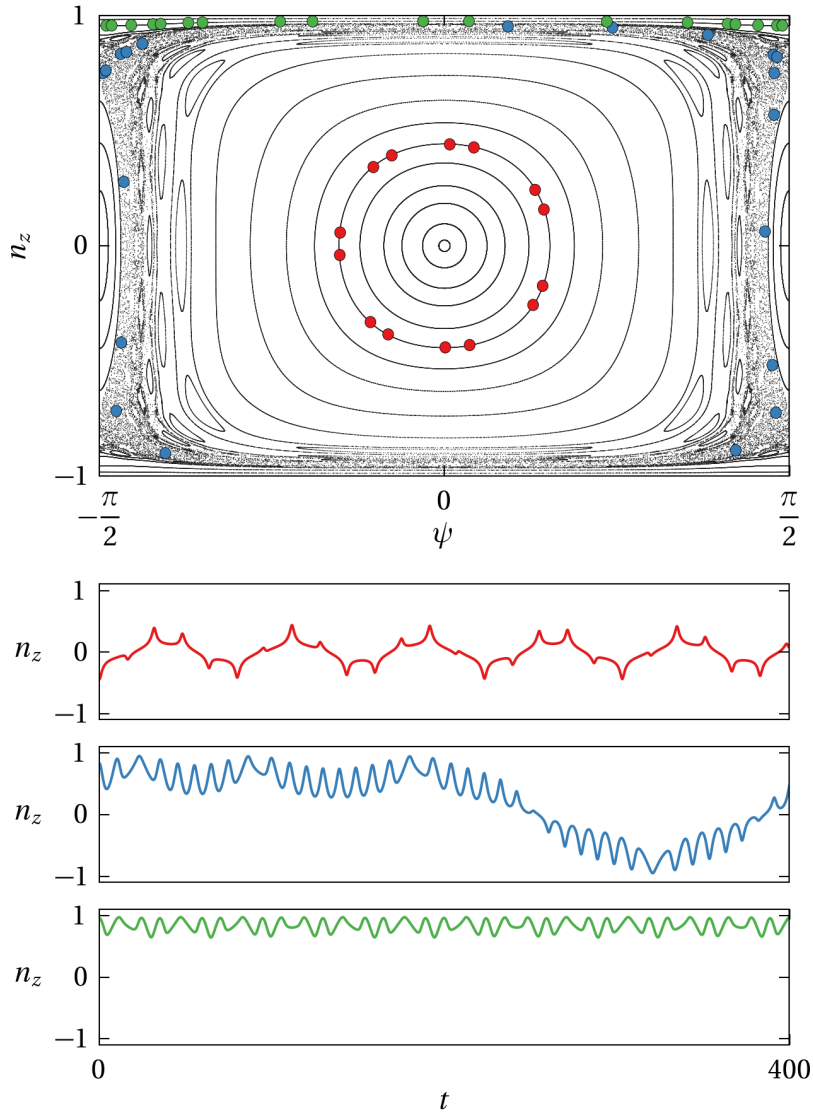

Figure 3.12: Top: Poincaré surface-of-section of an axisymmetric particle with aspect ratios $\lambda = 5$, $\kappa = 2$. Bottom: Examples of what $n_z(t)$ looks like, given the trajectory indicated by the color coded markers on the surface-of-section.

Men då mitt skarpsinne visade sig otillräckligt även för detta, slungade jag schackbrädet ut genom fönstret i huvudet på en gammal man med träben, för vilken döden endast var en välgärning, och kastade mig därefter ut i världsvimlet, föraktande mig själv.

ur *Spleen*, av Hjalmar Söderberg

Part II
My work

In the following three Sections I give the context and main results of my recent work.

In Section 4 I describe the development of an effective equation of motion for the orientation of a neutrally buoyant spheroid suspended in a simple shear flow, valid when inertial effects are weak but not vanishing. In short, we calculate what happens to the Jeffery orbits when the particle Reynolds number is non-zero. The results are contained in the appended Papers A-D.

The other two studies also relate to the orientational motion of non-spherical particles, and their common denominator is that they involve Jeffery's theory for ellipsoidal particles. The first, in Section 5, is a microfluidic experiment aiming to validate Jeffery's theory for the rotation of triaxial particles in shear flow (Paper E). The second, in Section 6, is a description of the rotational modes of small disks and rods in isotropic turbulence, combining data from experiments, direct numerical simulations and random flow theory (Paper F).

4 Effects of inertia on the Jeffery orbits

This project is a collaboration with collegues in Cherbourg and Marseille (France), and Stockholm (Sweden). J.R. Angilella (Cherbourg) and F. Candelier (Marseille) have many years of experience in dynamical systems, fluid mechanics and perturbation theory, without which this project would not have landed. T. Rosén and F. Lundell in Stockholm are experts in direct numerical simulation of particulate flows by the lattice Boltzmann method, by which we could validate our calculations. I also attribute the initial idea to perform stability analysis on the log-rolling motion under inertial perturbation, however vague at the time, to F. Lundell at a COST meeting in Udine, Italy.

Paper A is a brief summary of the calculation and result in letter form, while the Papers B & C contain all details. Paper D describes the direct numerical simulations that validate our theoretical calculation, and show in detail when the effective equations break down due to finite domain size and increasing importance of inertial effects.

4.1 History of problem

The Jeffery equations for an axisymmetric particle in simple shear flow are interesting because their solutions are degenerate, as explained in Section 3.5.1. Their solutions form a one-parameter family of periodic orbits. No orbit is preferred over another, so that the initial condition determines the dynamics indefinitely. Jeffery was very aware of this fact, he writes "It is obviously undesirable to leave a problem, which is physically quite determinate, in this indeterminate form." He further conjectures that "this failure is due to the limitations of the theory of the slow motion of a viscous fluid." In other words, he believed that inertial corrections were necessary to break the degenaracy. He concludes, referring to inertial corrections, "[...] a more complete investigation would reveal the fact that the particles do tend to adopt special orientations..." In connection with this discussion Jeffery hypothesized that this preferred orientation would be such that the energy dissipated by viscosity is minimized: a prolate particle ends up log-rolling (long axis along the vorticity), and an oblate particle tumbles (with a diameter along vorticity.)

Saffman [35] made the first attempt to include the non-linear inertial terms. It seems, although details are sparse, that he used an early form of asymptotic matching. For this he acknowledges I. Proudman, who a year later co-authored a paper [36] on the inertial correction to the drag on a translating sphere, pioneering the use of asymptotic matching in viscous fluid mechanics. But Saffman did not have the proper solution to the outer "Oseen problem" for matching, instead he invented a plausible but ad-hoc boundary condition to match the inner expansion. With this method, applied for nearly spherical particles, he found agreement with Jeffery's minimum dissipation hypothesis.

Harper & Chang [37] analyzed the rotation of two spheres rigidly constrained by an invisible rod, a so-called dumbbell. In the purely viscous regime a dumbell is equivalent to a prolate spheroid when its aspect ratio

approaches infinity. They assumed that both spheres experienced lift forces (calculated by Saffman [38]) independently of each other. By this method they found the opposite of Jeffery's minumum dissipation hypothesis: a slender rod ends up tumbling end-to-end in the flow-shear plane.

More recently Subramanian & Koch [33, 34] re-examined the slender rod and nearly-spherical limiting cases using a reciprocal theorem [16, 39]. Their method is less controversial than those employed by the earlier attemps. However, they found, like Harper & Chang [37], that for small values of the Reynolds number a slender rod tumbles end-to-end in the flow-shear plane. For larger values of the Reynolds number the tumbling orbit is destroyed and replaced by fixed points, which means that the particle stops rotating and aligns, a phenomenen observed in numerical studies [40] (see below). Subramanian & Koch [34] found that a nearly spherical prolate particle aligns its long axis along the vorticity, and a nearly spherical oblate particle tumbles, in agreement with Saffman [35]. They remark that the different types of motions for nearly spherical prolate particles, and slender prolate particles "suggests a possible bifurcation [...] at an intermediate aspect ratio."

Meanwhile, several groups began studies of this problem using direct numerical solution of the Navier-Stokes equations, via lattice Boltzmann simulations [40–48]. These studies reveal a rich structure of dynamical modes for moderate to large values of the Reynolds number. Not only log-rolling or tumbling is possible, but also intermediate limit cycles and alignment with new fixed points. The studies are limited to a few particle shapes, typically $\lambda = 1/4$, $\lambda = 1/2$, $\lambda = 2$ and $\lambda = 4$. Instead they focus on the effects of increasing Reynolds numbers, confinement and particle buoyancy.

I enter this chronology sometime in 2013, after submitting a paper [49] in which we describe the effects of particle inertia alone, neglecting the fluid inertia. We were intrigued by the results of Subramanian & Koch [33, 34] outlined above, and the fact that no numerical results had shown the predicted log-rolling mode for nearly spherical prolate particles. For example, Qi & Luo [42] simulated both oblate ($\lambda = 1/2$) and prolate ($\lambda = 2$) spheroids, and found for that the oblate particle log-rolls while the prolate particle tumbles, opposite to the existing theoretical prediction. But, as Subramanian & Koch [34] points out, there were several possible explanations for this discrepancy. First, the simulations were performed at moderately small Reynolds numbers, but not much smaller than unity, where a perturbation theory should be valid. Second, they were performed in a finite computational domain,

whereas the theory is valid for an unbounded shear flow. Third, the particle aspect ratio $\lambda = 2$ is not close to unity, whereas the theory assumed $\lambda \approx 1$. The parameter ranges where the existing theory should be valid is also where the numerical simulations become computationally impractical. More precisely, small values of the Reynolds number, large distance to the boundaries, and extreme particle shape all add to the computational cost. Therefore any comparisons to existing theory were qualitative.

These facts convinced us to attempt relaxing the assumption of $\lambda \approx 1$, and find the exact value of λ for the cross-over from log-rolling to tumbling.

During my work several more numerical studies have appeared [45–48]. Despite improved methods and more raw computer power, there was still no evidence of log-rolling prolate spheroids at small values of the Reynolds number. The clearest example is in Fig. 12 of Mao & Alexeev [46], where they find that the dynamics of a nearly spherical particle ($\lambda = 1.2$ and $\lambda = 0.8$) also contradicts the theoretical prediction. Their belief is that this "may be caused by the influence of the higher-order effects...", implying that the value of the Reynolds number in their simulation was out-of-range for the perturbation theory.

4.2 Results

We initially set out to calculate only the linear stability exponents of the log-rolling position. But it turned out that we could compute an explicit correction to Jeffery's equation of motion, which is more useful. Let $\boldsymbol{n}$ be the unit vector along the symmetry axis of the particle, and $\mathbb{O}$ and $\mathbb{S}$ the antisymmetric and symmetric parts of the shear flow gradient (see Section 3.1.1 for details.) Then the result is

$$\begin{aligned} \dot{\boldsymbol{n}} &= \mathbb{P}[\mathbb{O}\boldsymbol{n} + \Lambda\mathbb{S}\boldsymbol{n}] \\ &\quad + \mathrm{Re}_s \mathbb{P}[b_1(\boldsymbol{n}\cdot\mathbb{S}\boldsymbol{n})\mathbb{S}\boldsymbol{n} + b_2(\boldsymbol{n}\cdot\mathbb{S}\boldsymbol{n})\mathbb{O}\boldsymbol{n} + b_3\,\mathbb{O}\mathbb{S}\boldsymbol{n} + b_4\,\mathbb{S}\mathbb{S}\boldsymbol{n}]\,. \end{aligned} \tag{4.1}$$

Here the first row is the result of Jeffery [2]. The projection matrix $\mathbb{P} = \mathbb{1} - \boldsymbol{n}\boldsymbol{n}^{\mathrm{T}}$ removes any component of the vector field which is not tangent to the unit sphere (see also Section 3.5.) The scalar parameters Λ and b_α depend only on the particle aspect ratio λ. The shape factor $\Lambda = (\lambda^2 - 1)/(\lambda^2 + 1)$ was computed by Jeffery. Our main accomplishment is the calculation of $b_\alpha(\lambda)$.

The result (4.1) resolves the inconsistensies between earlier theories, and between theory and numerical simulations. It also conclusively refutes Jeffery's minimum dissipation hypothesis with respect to inertia. I summarise the main conclusions in the following.

Linear stability analysis

The solution to Jeffery's equation, Eq. (4.1) with $\mathrm{Re}_s = 0$, are the degenerate periodic Jeffery orbits. In terms of the dynamical system (4.1) the phase space S^2 is covered by a continuous family of marginally stable periodic orbits. But just as Jeffery conjectured, an arbitrarily small amount of inertia breaks this degeneracy. The periodic orbits in phase space are replaced by a set of limit cycles and fixed points. The stable limit cycles and fixed points of (4.1) represent the preferred motions of the particle. The form of Eq. (4.1) reveals that the vorticity direction $n_i \sim \varepsilon_{ijk} O_{jk}$ is a fixed point, whatever the values of $\beta_\alpha(\lambda)$. This fixed point is called *log-rolling*. Similarly, no trajectory of Eq. (4.1) can cross the flow-shear plane, and therefore the phase space in that plane must contain either a limit cycle, or a set of fixed points. If it is a limit cycle, the dynamics is called *tumbling*. These general features are due to the symmetries of the shear flow and the axisymmetric particle.

First effects of inertia

For an arbitrarily small value of $\mathrm{Re}_s > 0$ the phase space looks almost like the Jeffery orbits, but with a slow *drift* between the orbits. This drift is bounded by the log-rolling and tumbling orbits, and the direction of the drift is determined by the particle shape. We determine the drift by linear stability analysis of Eq. (4.1) to order $O(\mathrm{Re}_s)$, and find

- $1 < \lambda < \infty$ (prolate): The particle drifts to the stable tumbling limit cycle, whatever the initial condition.
- $1/7.3 \approx \lambda_c < \lambda < 1$ (thick oblate): The particle drifts to the stable log-rolling fixed point, whatever the initial condition.
- $0 < \lambda < \lambda_c$ (thin oblate): Both the log-rolling fixed point and the tumbling limit cycle are stable. Their basins of attraction are separated by one of the intermediate Jeffery orbits which have turned into an

unstable limit cycle. The position of the unstable limit cycle depends on the particle shape, shown in Fig. 4 of Paper C.

Our result (4.1) agrees with those of Subramanian & Koch [33] in the limit $\lambda \to \infty$ (up to a factor of 8π). However, we find that the earlier results for nearly spherical particles [34, 35] are mistaken. We have checked this in two ways. First, with F. Candelier we analysed the case of nearly spherical particles by a simultaneous perturbation around $\mathrm{Re}_s = 0$ and $\lambda = 1$. We regard this complementary calculation as technically independent, because the flow solutions are expressed in spherical harmonics instead of a singularity system, and it does not use the symmetry arguments we put forward for the general case. This calculation, due mostly to F. Candelier, is described in Paper B. We knew that my general solution must match this special solution for nearly spherical particles exactly, as $\lambda \to 1$. Once we established this equivalence we compared my solution to Subramanian & Koch [33] as $\lambda \to \infty$, and found agreement up to a numerical factor of 8π. We have not identified exactly where in their calculation this factor appears, but the likely culprit is in the definition of Green's functions for the Stokes flow (see App. A.2 in Paper C.) With these comparisons we were confident enough to submit our calculations for review and publication. The second check of our result is the direct numerical stability analysis by T. Rosén and F. Lundell. Our effective equation (4.1) agrees very well with the full numerical solution as $\mathrm{Re}_s \to 0$ and the computational box size becomes large. This comparison is in Paper D (in particular Fig. 2). We conclude that our effective equation is correct. But we also see that the orientational dynamics of a non-spherical particle in shear flow is sensitive to both confinement (wall-effects), and to higher-order corrections in the shear Reynolds number.

Dynamics of oblate particles at finite values of Re_s

In the previous Section I discussed the effects of inertia when Re_s is arbitrarily small, but not zero. In this limit we expect the perturbative effective equation (4.1) to be valid. For larger values of Re_s we cannot be certain that the dynamics of the effective equation reflects the dynamics of the exact equations. For example, the effective equation can in general not predict at which value of Re_s a disk-shaped particle with $\lambda = 1/12$ will cease rotating. Nevertheless, we may construct a bifurcation diagram of the effective equation in the parameter space (λ, Re_s). We know that any bifurcation line

that extends to $\mathrm{Re}_s = 0$ in the parameter space of the effective equation must *connect* to a corresponding bifurcation line in the parameter space of the exact dynamics. This constrains the possible bifurcation topologies for the exact equations, and may serve as a guide for further numerical analysis.

Three bifurcation lines in the parameter space of the effective equation extend to $\mathrm{Re}_s = 0$. Two of them describe the value of Re_s where the tumbling orbit ceases to exist and is replaced by a pair of fixed points. Those reach $\mathrm{Re}_s = 0$ only asymptotically as $\lambda \to 0$ and $\lambda \to \infty$, corresponding to infinitely thin disks or rods. The slender-body limit was described by Subramanian & Koch [33]. The third bifurcation line separates the regions of stable and unstable tumbling for oblate particles, referred to in the previous Section. It connects to $\mathrm{Re}_s = 0$ at $\lambda = \lambda_c \approx 1/7.3$. In Paper D there is numerical evidence that this happens also in the exact equations. This raises the question: where does this bifurcation line go as Re_s increase in the effective equation? To answer this question I show the bifurcation diagram for oblate particles in Fig. 4.1. The interesting feature of this diagram is the fate of the tumbling orbit bifurcation. It meets several other bifurcation lines in a "critical point" (marked by a red circle in Fig. 4.1). For even larger values of Re_s there may exist more bifurcations (not shown), but I expect them to be less relevant.

Numerical simulation of the exact equations reveals many different modes of rotation, depending on parameters such as particle aspect ratio, Reynolds number, confinement ratio and particle buoyancy. One may hope that the effective equation is qualitatively correct in predicting what the first bifurcation is as Re_s increases. The data of Rosén *et al.* [48] and Paper D indicate that the "critical point", where several bifurcation lines merge, does exist also in the exact dynamics. However, the bifurcation lines seem to be sensitive to the confinement ratio in the numerical simulations and as of now we do not have enough data to confirm nor refute any claims on equivalence.

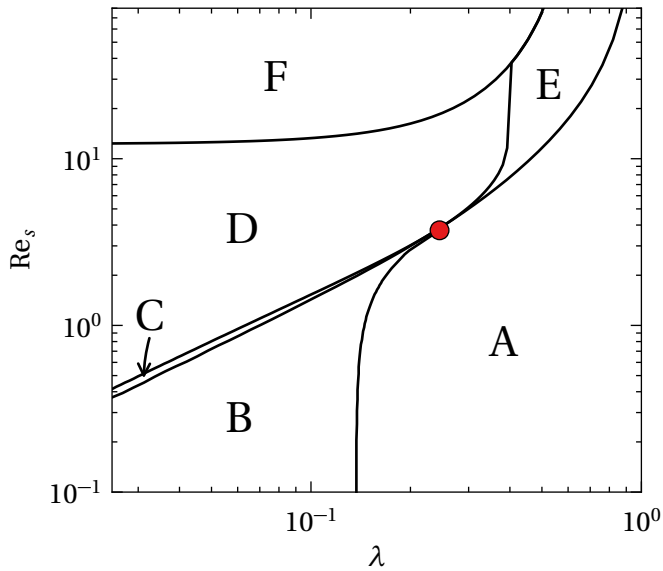

Figure 4.1: Bifurcation diagram for oblate particles ($\lambda < 1$) in the effective equations (4.1). Log-rolling is stable everywhere in this phase diagram. Regions:

A - Tumbling orbit unstable,
- No additional fixed points/orbits exist.

B - Tumbling orbit stable,
- Limit cycle separates basins of attraction of log rolling and tumbling.

C - Fixed points replace tumbling orbit: one saddle, one stable node,
- Limit cycle separates basins of attraction of log rolling and tumbling.

D - Fixed points replace tumbling orbit: one unstable node, one stable node,
- Saddle point exists in interior near tumbling fixed points.

E - Fixed points replace tumbling orbit: one unstable node, one saddle,
- No additional fixed points/orbits exist.

F - Two new fixed points are created, in total four fixed points exist in place of the tumbling orbit.

For larger values of Re_s there may exist more bifurcations (not shown).

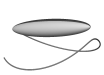

5 Measurements of asymmetric rods tumbling in microchannel flow

5.1 Overview

This project is a collaboration with our experimentalist collegues in Gothenburg, Sweden. Roughly the division of work is that they build and perform the experiment, and we design the specifications and perform the analysis.

The project was initiated with an intention of observing the scattering between Jeffery orbits due to thermal noise. But first we needed to observe plain Jeffery orbits, as a baseline. With hindsight that was naive, given the long list of skilled experimentalists before us who struggled with this: Sec. II in Paper E gives a more or less exhaustive list.

Our focus has shifted away from thermal noise, to the sensitive dependence on particle shape and initial condition. In Section 3.5.2 in Part I, I explained how Jeffery's result implies complicated dynamics for triaxial particles, even if the deviation from axisymmetry very small [28, 29]. We want to observe this effect in experiment.

We previously published two papers [50, 51] describing our methods and some initial observations. In Paper E we describe our most recent measurements. We are still using pressure-driven flow in a microchannel molded in PDMS plastic (Fig. 5.1), but there are two main technical improvements from earlier work. First, we employ an optical trap to arrange particles for the experimental runs. This allows us to use the same particle several times, and to control its initial condition. Second, we have particles made from glass rods which have a very symmetric cross-section (see Fig. 2 in Paper E).

In Paper E we claim to observe both quasi-periodic and chaotic trajectories, for the same particle. Thus we confirm the predictions of Hinch & Leal [28] and Yarin *et al.* [29]. We claim that the observed trajectories are due to the triaxial particle shape for two reasons.

First, we reverse the pressure over the channel at the end of each particle trajectory. In the Stokes approximation the particle must then retrace its trajectory backwards, in line with the time-reversal symmetry of the Jeffery equations discussed in Section 3.5. If the particle trajectory does not reverse we discard the data. These reversals exclude any non-reversible effects, in

Figure 5.1: Photograph of a microchannel of the type used in our experiment. The channel is molded in a block of PDMS plastic. In the picture the channel is filled with dye. To the left and right are inlet/outlet tubes. The channel is approximately 5 cm long.

particular effects of inertia or thermal noise.

Second, with each particle we record several distinct trajectories with different initial conditions. This enables comparison with theory despite the fact that we cannot determine the particle shape accurately, because we know that all trajectories for the same particle must be consistent with the same surface-of-section of the Jeffery dynamics (see Section 3.5.2). A complication is that we cannot measure the rotation of the rod around its long axis, that is the angle ψ in the surface-of-section. However, the elliptic-island structure of the surface-of-section makes a comparison with the measured values of n_z meaningful, because the dynamics are strongly influenced by the initial condition and the size of the island bounds the oscillations of n_z for any trajectory.

6 Rotation rates of particles in turbulence

Paper F started as the synthesis of discussions during a workshop at NORDITA in Stockholm. For those I am grateful especially to E. Variano and G. Voth. The paper is a discussion of the rotations of axisymmetric particles in isotropic turbulence. I think the strength of this paper is it's breadth, as it contains pieces of experimental results, numerical results and analytical model calculations.

From what I remember, the discussions started because of confusion between the *rotation rate* and the *tumbling rate* of a particle. In this context rotation rate means magnitude of the angular velocity: $|\boldsymbol{\omega}|$. The tumbling rate is the rate at which the symmetry axis of the particle turns: $|\dot{\boldsymbol{n}}| = |\boldsymbol{\omega} \times \boldsymbol{n}|$. The two are kinematically related, because

$$|\boldsymbol{\omega}|^2 = |\dot{\boldsymbol{n}}|^2 + |\boldsymbol{\omega} \cdot \boldsymbol{n}|^2 . \tag{6.1}$$

The difference $|\boldsymbol{\omega} \cdot \boldsymbol{n}|$ is called the *spinning rate*, because it is the rate at which the particle spins around its symmetry axis.

In the paper we make two main observations. First, that the average rotation rate is roughly independent of particle shape. This is true in numerical simulations (Fig. 3 in Paper F), and in experimental measurements (Fig. 5 in Paper F.) This shape independence is unexpected, in particular because the average tumbling rate has a strong shape dependence [26, 52]. Therefore it turns out that the shape dependence of the average spinning rate almost exactly cancels the shape dependence of the average tumbling rate, as to make the total rotation rate shape independent. The reasons for this cancellation are still not known. However, in the paper we show that the average rotation rate of a particle in a random flow field is *not* shape independent. This implies that the cancellation is due to the properties of the turbulent flow, and not inherent in the equations of motion.

The second main observation is on the *instantaneous* rotation rates of particles. Although the average rotation rates for a thin disk and a slender rod are almost the same, their trajectories are qualitatively very different.

A key feature of turbulence is the existence of *vortex tubes* [53]. They are regions of strong vorticity, created by stretching of a large vortex into a thinner but more intensive vortex. These regions typically are long-lived, compared to the average rate of change in the flow. In these vortex tubes rod-shaped particles tend to rotate such that they keep aligned with the direction of the vorticity. The vorticity makes them spin around their own symmetry axis. But disks instead align perpendicularly to the vorticity, and the vorticity makes them tumble. But as a disk tumbles, the tumbling rate alternates between being faster and slower than vorticity, because of the flow strain. An example of this is shown in the first panel of Fig. 1 in Paper F. The rotation rate of the rod varies smoothly, and is very close to the strength of the vorticity. The rotation rate of the disk oscillates strongly, but is on average close to the strength of the vorticity.

We may partly understand these observations by a simplified picture. The effect of a rotational flow $\boldsymbol{u}_R = \boldsymbol{\Omega} \times \boldsymbol{r}$ is to rotate a particle around $\boldsymbol{\Omega}$. The effect of a strain flow $\boldsymbol{u}_S = \mathbb{S}\boldsymbol{r}$ is to align a long axis of a particle with the strongest eigendirection of $\mathbb{S}$. The simple picture is that the same strain that stretches and intensifies a vortex to a vortex tube along $\boldsymbol{\Omega}$, will also align the axes of any nearby particles with $\boldsymbol{\Omega}$. Therefore long axes of rods, and diameters of disks tend to align with $\boldsymbol{\Omega}$ in these regions. With this alignment it follows that rods spin and disks tumble because of the strong vorticity.

This simple argument cannot explain why the rotation rate of the disk happens to average to the same value as that of the rod. The details of the tumbling rate depends on how the vorticity $\boldsymbol{\Omega}$, and the particle direction $\boldsymbol{n}$, are aligned relative to the eigensystem of $\mathbb{S}$. The details and implications of these alignments are important open questions. In the random-flow model these alignments are very weak, and that is the underlying reason for the shape-dependence of the average rotation rate.

7 Closing words

The past five years have been an immense learning experience for me. I was fortunate to come to Bernhard Mehlig's group around 2010. They had been working on the dynamics of particles in random flows for some time, and were increasingly interested in the theory of fluid mechanics underlying the equations of motion. I got the job as a Ph.D student, and my new job was to learn, which is a fantastic job description.

Five years later I can say that I surely learned some fluid mechanics and mathematics, but more importantly I learned about intellectual independence. I learned that independent thought requires *knowing what you don't know.* It seems trivial that we should not accept, or worse, repeat, arguments that we do not understand. In my experience I am nevertheless tempted to accept an argument because I find the conclusion attractive. The most important skill I learned is to recognize and fight this temptation within myself.

During this time we also made some scientific progress, documented in Part II of this thesis and the appended papers. I end this thesis with a brief discussion of those results, and their possible future extension.

7.1 Discussion of results

Personally, the most satisfying result of my work is the description of the effect of inertia on the Jeffery orbits (Papers A-D). First, it resolves a rather long-standing problem in theoretical fluid mechanics. The degeneracy of the Jeffery orbits is well-known, and anyone in the field immediately understands the question. Second, the result offered a couple of surprises. While the established asymptotic results for nearly spherical particles motivated us to attempt the calculation (see Section 4), they turned out to be mistaken, and there is no bifurcation of the log-rolling orbit for rod-shaped particles. On the other hand we found a non-trivial bifurcation for oblate particles of intermediate aspect ratio that I believe no-one anticipated. The original assertion that the effects of inertia breaks the degeneracy is somewhat thwarted, as the dynamics of a thin oblate particle is determined by which basin of attraction it starts in. The fact that this theoretical prediction seems to agree with new direct numerical simulations is of course very satisfying.

The experiment described in Paper E has been a catalyst for me to dig into the dynamics of triaxial particles in shear flow. Our group has roots in research on dynamical systems, so from first sight Bernhard asked why the surfaces-of-section (Section 3.5.2) look like those of the Hamiltonian 'standard map'? Eventually, with help from S. Östlund, we realized that the reversal symmetry we invoke in the analysis of the experiment must also imply a combined time-reversal and mirror symmetry in the equations of motion. This symmetry is not obvious in the Euler angle coordinates, because they cannot describe a mirror operation. But in the vector equations for $\boldsymbol{n}$ and $\boldsymbol{p}$ the symmetry is easily checked. In fact, I believe the symmetry should hold for any particle shape, because it is a consequence of Stokes equation.

Paper F is different because it concerns random and turbulent flows instead of a simple shear flow. For me it was a lot of fun discussing and writing this paper, as well as our earlier paper on the same topic [26], because I had to learn about the statistics of turbulent flow. The main complication with angular dynamics is that the torque on a particle depends on the orientation of the particle relative to the gradients. Several groups are at work measuring, simulating and understanding these correlations between the particle orientation and the fluid gradients in turbulence. This research will contribute to our understanding of both the particle dynamics and the dynamics of the turbulent gradients, and I like to think I made a contribution towards this.

7.2 Outlook

Experimental observations of angular dynamics in shear flow

There are two obvious extensions to this work, one theoretical and one experimental.

Experimentally the next step is to measure the complete three-dimensional orientation of the particle. This is very difficult with microrods, and therefore we investigate alternative particle shapes. For example it is possible to measure the orientation of a triangular platelet using only one camera, except for some degenerate orientations which have to be determined by continuity.

The theoretical question concerns how the surface-of-section is modified for asymmetric particles. The Jeffery equation is valid for any particle with three orthogonal mirror symmetries [20]. But the real particles in this experiment are not perfectly symmetric. The trajectories are sensitive to the transition from axisymmetric to triaxial, and the question is whether they are equally sensitive to breaking the mirror symmetries as well.

The effects of fluid inertia

The reason that the calculation described in Papers A-C is conceptually straightforward is that the Stokes flow works as the zeroth order flow field in the reciprocal theorem integral. Perturbation theory for small values of the Reynolds number is infamous, because the Stokes flow field is not a uniformly valid approximation of the flow field as $\mathrm{Re}_s \to 0$. This generally leads to a erronous or divergent result in perturbation theory. In our case this did not matter, because the erronous contribution to the volume integral of the reciprocal theorem is small. But in cases involving translational motion the volume integral diverges. We may not, for example, reproduce the Saffman lift force on a sphere translating in simple shear with just the Stokes flow field and the reciprocal theorem.

In order to solve most problems, it is necessary to construct uniformly valid flow fields to lowest order. This usually requires singular perturbation theory, of which asymptotic matching is perhaps the most common technique in fluid dynamics. Learning these methods is a necessary next step.

An interesting extension is to solve the coupled spatial and angular dy-

namics of a non-spherical particle in shear flow. To lowest order it makes sense to consider the rotation separately, because the Reynolds number based on the particle slip velocity is small compared to the shear Reynolds number. But at the next order of perturbation the rotation and translation are probably not decoupled. Such a calculation would be the analogue of the Saffman lift for non-spherical particles, and could make our results more relevant to inertial microfluidics.

Another effect neglected in our calculation is the effect of confinement of the particle by nearby walls. The nearby boundaries affect the nature of the inertial correction. Likely this effect can be computed similarly to the result in Paper C, with the method of images for the multipole expansion.

Finally, in my view, a long-term goal of this research is to understand how to derive an effective equation of motion for the translational and orientational dynamics of a neutrally buoyant particle in turbulence. The Stokes drag is a good approximation for very small particles, or for finite particles if they are much heavier than the fluid. But for a neutrally buoyant particle in turbulence I expect both particle inertia and fluid inertia to contribute to an effective equation of motion.

Blåsten visslar i fönsterspringorna, och regnet porlar i takrännan, och nu är sagan slut. Den som icke har förstått den kan trösta sig med att det blir vackert väder imorgon.

ur *Duggregnet*, av Hjalmar Söderberg

ACKNOWLEDGEMENTS

Although written by my hand, this thesis is by no means conceived by me alone. I am most grateful for the enthusiastic guidance from my supervisor Bernhard Mehlig. It is a privilege to work with someone with the physical insight, unquenchable enthusiasm and sheer perseverance it takes to get things right.

Further, I am indebted to all our collaborators for their work. Fabien Candelier and Jean-Régis Angilella in France for teaching me fluid dynamics. Greg Voth and Evan Variano in the US for the wonderful experiments and discussions, and our experimental collegues in Dag Hanstorp's lab for hunting the Jeffery orbits with us.

I also want to thank my present and former collegues for the open scientific environment at the department. In particular I appreciate the company of my fellow students Kristian Gustafsson, Marina Rafajlović and Erik Werner (who all graduated before me), and I welcome our new students Johan Fries and Jan Meibohm to this group. An extra thank you to Erik and Jan who improved this thesis with their helpful comments. Any remaining mistakes are mine alone.

Finally, I am fortunate to have my wonderful family. Thank you Freja and Tora for giving meaning to it all ♡.

Bibliography

[1] EINARSSON, J 2013 *Orientational dynamics of small non-spherical particles in fluid flows*. Gothenburg University, ISBN: 978-91-637-4473-0, https://gupea.ub.gu.se/handle/2077/34320.

[2] JEFFERY, G. B 1922 The motion of ellipsoidal particles immersed in a viscous fluid. *Proceedings of the Royal Society of London. Series A* **102** (715), 161–179.

[3] DEVENISH, B. J, BARTELLO, P, BRENGUIER, J. L, COLLINS, L. R, GRABOWSKI, W. W, IJZERMANS, R. H. A, MALINOWSKI, S. P, REEKS, M. W, VASSILICOS, J. C, WANG, L. P & WARHAFT, Z 2012 Droplet growth in warm turbulent clouds. *Quarterly Journal of the Royal Meteorological Society* **138** (667), 1401–1429.

[4] WILKINSON, M, MEHLIG, B & USKI, V 2008 Stokes trapping and planet formation. *The Astrophysical Journal Supplement Series* **176** (2), 484–496.

[5] GUASTO, J. S, RUSCONI, R & STOCKER, R 2012 Fluid mechanics of planktonic microorganisms. *Annual Review of Fluid Mechanics* **44** (1), 373–400.

[6] BAYOD, E, WILLERS, E. P & TORNBERG, E 2008 Rheological and structural characterization of tomato paste and its influence on the quality of ketchup. *LWT - Food Science and Technology* **41** (7), 1289–1300.

[7] COUSSOT, P, NGUYEN, Q. D, HUYNH, H. T & BONN, D 2002 Avalanche behavior in yield stress fluids. *Physical Review Letters* **88** (17), 175501.

[8] MATHER, T, PYLE, D & OPPENHEIMER, C 2003 Tropospheric volcanic aerosol. In *Volcanism and the Earth's Atmosphere* (ed. A Robock & C Oppenheimer), p. 189–212. American Geophysical Union.

[9] GASTEIGER, J, GROSS, S, FREUDENTHALER, V & WIEGNER, M 2011 Volcanic ash from Iceland over Munich: mass concentration retrieved from ground-based remote sensing measurements. *Atmos. Chem. Phys.* **11** (5), 2209–2223.

[10] DUBOVIK, O, HOLBEN, B. N, LAPYONOK, T, SINYUK, A, MISHCHENKO, M. I, YANG, P & SLUTSKER, I 2002 Non-spherical aerosol retrieval method employing light scattering by spheroids. *Geophysical Research Letters* **29** (10), 54–1.

[11] MARCOS, SEYMOUR, J. R, LUHAR, M, DURHAM, W. M, MITCHELL, J. G, MACKE, A & STOCKER, R 2011 Microbial alignment in flow changes ocean light climate. *Proceedings of the National Academy of Sciences* PMID: 21368125.

[12] SABINE, E 1829 On the reduction to a vacuum of Captain Kater's convertible pendulum. *Philosophical Transactions of the Royal Society of London* **119**, 331–338.

[13] STOKES, G. G 1851 On the effect of the internal friction of fluids on the motion of pendulums. *Transactions of the Cambridge Philosophical Society* **IX**, 8, reprinted in Cambridge Library Collection: Mathematical and Physical Papers Vol. 3. ISBN 9780511702266.

[14] VEYSEY, J & GOLDENFELD, N 2007 Simple viscous flows: From boundary layers to the renormalization group. *Reviews of Modern Physics* **79** (3), 883–927.

[15] BRENNER, H 1974 Rheology of a dilute suspension of axisymmetric Brownian particles. *International Journal of Multiphase Flow* **1** (2), 195–341.

[16] KIM, S & KARRILA, S. J 1991 *Microhydrodynamics: principles and selected applications*. Boston: Butterworth-Heinemann.

[17] HAPPEL, J. R & BRENNER, H 1965 *Low Reynolds Number Hydrodynamics: With Special Applications to Particulate Media*. Springer.

[18] CLERCX, H. J. H & SCHRAM, P. P. J. M 1992 Brownian particles in shear flow and harmonic potentials: A study of long-time tails. *Physical Review A* **46** (4), 1942–1950.

[19] KHEIFETS, S, SIMHA, A, MELIN, K, LI, T & RAIZEN, M. G 2014 Observation of Brownian Motion in Liquids at Short Times: Instantaneous Velocity and Memory Loss. *Science* **343** (6178), 1493–1496.

[20] BRENNER, H 1964 The Stokes resistance of an arbitrary particle—II. *Chemical Engineering Science* **19** (9), 599–629.

[21] BRENNER, H & O'NEILL, M. E 1972 On the Stokes resistance of multiparticle systems in a linear shear field. *Chemical Engineering Science* **27** (7), 1421–1439.

[22] OBERBECK, A 1876 Uber stationäre flüssigkeitsbewegungen mit berücksichtigung der inneren reibung. *Journal für die reine und angewandte Mathematik* **81**, 62–80.

[23] EDWARDES, D 1893 Steady motion of a viscous liquid in which an ellipsoid is constrained to rotate about a principal axis. *The quarterly journal of pure and applied mathematics* **26**, 70–78.

[24] BRETHERTON, F. P 1962 The motion of rigid particles in a shear flow at low reynolds number. *Journal of Fluid Mechanics* **14** (02), 284–304.

[25] LAMB, J. S. W & ROBERTS, J. A. G 1998 Time-reversal symmetry in dynamical systems: A survey. *Physica D: Nonlinear Phenomena* **112** (1–2), 1–39.

[26] GUSTAVSSON, K, EINARSSON, J & MEHLIG, B 2014 Tumbling of small axisymmetric particles in random and turbulent flows. *Physical Review Letters* **112** (1), 014501.

[27] GIERSZEWSKI, P. J & CHAFFEY, C. E 1978 Rotation of an isolated triaxial ellipsoid suspended in slow viscous flow. *Canadian Journal of Physics* **56** (1), 6–11.

[28] HINCH, E. J & LEAL, L. G 1979 Rotation of small non-axisymmetric particles in a simple shear flow. *Journal of Fluid Mechanics* **92** (03), 591–607.

[29] YARIN, A. L, GOTTLIEB, O & ROISMAN, I. V 1997 Chaotic rotation of triaxial ellipsoids in simple shear flow. *Journal of Fluid Mechanics* **340**, 83–100.

[30] GOLDSTEIN, H 1980 *Classical Mechanics*. Reading, Massachusetts: Addison-Wesley.

[31] STROGATZ, S. H 1994 *Nonlinear dynamics and Chaos*. Westview Press.

[32] LUNDELL, F 2011 The effect of particle inertia on triaxial ellipsoids in creeping shear: From drift toward chaos to a single periodic solution. *Physics of Fluids* **23** (1), 011704.

[33] SUBRAMANIAN, G & KOCH, D. L 2005 Inertial effects on fibre motion in simple shear flow. *Journal of Fluid Mechanics* **535**, 383–414.

[34] SUBRAMANIAN, G & KOCH, D. L 2006 Inertial effects on the orientation of nearly spherical particles in simple shear flow. *Journal of Fluid Mechanics* **557**, 257–296.

[35] SAFFMAN, P. G 1956 On the motion of small spheroidal particles in a viscous liquid. *Journal of Fluid Mechanics* **1** (05), 540–553.

[36] PROUDMAN, I & PEARSON, J. R. A 1957 Expansions at small Reynolds numbers for the flow past a sphere and a circular cylinder. *Journal of Fluid Mechanics* **2** (03), 237–262.

[37] HARPER, E. Y & CHANG, I.-D 1968 Maximum dissipation resulting from lift in a slow viscous shear flow. *Journal of Fluid Mechanics* **33** (02), 209–225.

[38] SAFFMAN, P. G 1965 The lift on a small sphere in a slow shear flow. *Journal of Fluid Mechanics* **22** (02), 385–400.

[39] LOVALENTI, P. M & BRADY, J. F 1993 The hydrodynamic force on a rigid particle undergoing arbitrary time-dependent motion at small Reynolds number. *Journal of Fluid Mechanics* **256**, 561–605.

[40] DING, E.-J & AIDUN, C. K 2000 The dynamics and scaling law for particles suspended in shear flow with inertia. *Journal of Fluid Mechanics* **423**, 317–344.

[41] FENG, J & JOSEPH, D. D 1995 The unsteady motion of solid bodies in creeping flows. *Journal of Fluid Mechanics* **303**, 83–102.

[42] QI, D & LUO, L.-S 2003 Rotational and orientational behaviour of three-dimensional spheroidal particles in couette flows. *Journal of Fluid Mechanics* **477**, 201–213.

[43] YU, Z, PHAN-THIEN, N & TANNER, R. I 2007 Rotation of a spheroid in a couette flow at moderate reynolds numbers. *Physical Review E* **76** (2), 026310.

[44] HUANG, H, YANG, X, KRAFCZYK, M & LU, X.-Y 2012 Rotation of spheroidal particles in couette flows. *Journal of Fluid Mechanics* **692**, 369–394.

[45] ROSÉN, T, LUNDELL, F & AIDUN, C. K 2014 Effect of fluid inertia on the dynamics and scaling of neutrally buoyant particles in shear flow. *Journal of Fluid Mechanics* **738**, 563–590.

[46] MAO, W & ALEXEEV, A 2014 Motion of spheroid particles in shear flow with inertia. *Journal of Fluid Mechanics* **749**, 145–166.

[47] ROSÉN, T, DO-QUANG, M, AIDUN, C. K & LUNDELL, F 2015 The dynamical states of a prolate spheroidal particle suspended in shear flow as a consequence of particle and fluid inertia. *Journal of Fluid Mechanics* **771**, 115–158.

[48] ROSÉN, T, DO-QUANG, M, AIDUN, C. K & LUNDELL, F 2015 Effect of fluid and particle inertia on the rotation of an oblate spheroidal particle suspended in linear shear flow. *Physical Review E* **91** (5).

[49] EINARSSON, J, ANGILELLA, J. R & MEHLIG, B 2014 Orientational dynamics of weakly inertial axisymmetric particles in steady viscous flows. *Physica D: Nonlinear Phenomena* **278–279**, 79–85.

[50] MISHRA, Y. N, EINARSSON, J, JOHN, O. A, ANDERSSON, P, MEHLIG, B & HANSTORP, D 2012 A microfluidic device for studies of the orientational dynamics of microrods. In *Proc. SPIE*, , vol. 8251, pp. 825109–825109–11.

[51] EINARSSON, J, JOHANSSON, A, MAHATO, S. K, MISHRA, Y. N, ANGILELLA, J. R, HANSTORP, D & MEHLIG, B 2013 Periodic and aperiodic tumbling of microrods advected in a microchannel flow. *Acta Mechanica* **224** (10), 2281–2289.

[52] PARSA, S, CALZAVARINI, E, TOSCHI, F & VOTH, G. A 2012 Rotation rate of rods in turbulent fluid flow. *Physical Review Letters* **109** (13), 134501.

[53] SHE, Z.-S, JACKSON, E & ORSZAG, S. A 1990 Intermittent vortex structures in homogeneous isotropic turbulence. *Nature* **344** (6263), 226–228.

APPENDIX

A Triaxial particle in a linear flow

In this Appendix I derive the torque-free equation of motion for an triaxial ellipsoidal particle in a general linear flow. It is the generalisation of the Jeffery equation to triaxial particles.

We represent the orientation of the particle with a rotation matrix $\mathbb{R}(t)$, which transforms the world-fixed cartesian coordinate frame $(\boldsymbol{e}_1, \boldsymbol{e}_2, \boldsymbol{e}_3)$ to the particle-fixed coordinate frame $(\boldsymbol{n}_1, \boldsymbol{n}_2, \boldsymbol{n}_3)$. The ellipsoid is defined by the lengths of its three half-axes, we denote them a_1, a_2 and a_3. Each a_i is the length along the corresponding particle axis $\boldsymbol{n}_i$.

The end result of this calculation is an equation of motion for $\boldsymbol{n}_1$ and $\boldsymbol{n}_2$. The two orthogonal vectors describe fully the orientation of the rigid body.

The kinematic equation of motion for a rotating vector is

$$\dot{\boldsymbol{n}}_i = \boldsymbol{\omega} \times \boldsymbol{n}_i, \tag{A.1}$$

where $\boldsymbol{\omega}$ is the angular velocity of the particle. Jeffery [2] computed the components of the angular velocity vector in the particle frame of reference. Updated to the present notation, his Eq. (37) reads

$$\begin{aligned}
(\boldsymbol{n}_1 \cdot \boldsymbol{\omega}) &= \boldsymbol{n}_1 \cdot \boldsymbol{\Omega} + \frac{a_2^2 - a_3^2}{a_2^2 + a_3^2} \left(\boldsymbol{n}_2^{\mathrm{T}} \mathbb{S} \boldsymbol{n}_3 \right), \\
(\boldsymbol{n}_2 \cdot \boldsymbol{\omega}) &= \boldsymbol{n}_2 \cdot \boldsymbol{\Omega} + \frac{a_3^2 - a_1^2}{a_3^2 + a_1^2} \left(\boldsymbol{n}_3^{\mathrm{T}} \mathbb{S} \boldsymbol{n}_1 \right), \\
(\boldsymbol{n}_3 \cdot \boldsymbol{\omega}) &= \boldsymbol{n}_3 \cdot \boldsymbol{\Omega} + \frac{a_1^2 - a_2^2}{a_1^2 + a_2^2} \left(\boldsymbol{n}_1^{\mathrm{T}} \mathbb{S} \boldsymbol{n}_2 \right).
\end{aligned}$$

Here $\boldsymbol{\Omega}$ is such that $\boldsymbol{\Omega} \times x = \mathbb{O}\boldsymbol{x}$, where $\mathbb{S}$ and $\mathbb{O}$ are the symmetric and anti-symmetric parts of the flow gradient:

$$\mathbb{O} = \frac{1}{2}(\mathbb{A} - \mathbb{A}^{\mathrm{T}}), \quad \mathbb{S} = \frac{1}{2}(\mathbb{A} + \mathbb{A}^{\mathrm{T}}), \quad \mathbb{A} = \nabla \boldsymbol{u} = \mathbb{O} + \mathbb{S}.$$

We can put Jeffery's expression into a single vector expression

$$\boldsymbol{\omega} = \boldsymbol{\Omega} + \frac{a_2^2 - a_3^2}{a_2^2 + a_3^2}\left(\boldsymbol{n}_2^{\mathrm{T}}\mathbb{S}\boldsymbol{n}_3\right)\boldsymbol{n}_1 + \frac{a_3^2 - a_1^2}{a_3^2 + a_1^2}\left(\boldsymbol{n}_3^{\mathrm{T}}\mathbb{S}\boldsymbol{n}_1\right)\boldsymbol{n}_2 + \frac{a_1^2 - a_2^2}{a_1^2 + a_2^2}\left(\boldsymbol{n}_1^{\mathrm{T}}\mathbb{S}\boldsymbol{n}_2\right)\boldsymbol{n}_3.$$

In order to ease the notation we introduce the two aspect ratios $\lambda = a_3/a_1$ and $\kappa = a_2/a_1$:

$$\boldsymbol{\omega} = \boldsymbol{\Omega} + \frac{\Lambda - K}{K\Lambda - 1}\left(\boldsymbol{n}_2^{\mathrm{T}}\mathbb{S}\boldsymbol{n}_3\right)\boldsymbol{n}_1 + \Lambda\left(\boldsymbol{n}_3^{\mathrm{T}}\mathbb{S}\boldsymbol{n}_1\right)\boldsymbol{n}_2 - K\left(\boldsymbol{n}_1^{\mathrm{T}}\mathbb{S}\boldsymbol{n}_2\right)\boldsymbol{n}_3,$$

where

$$K = \frac{\kappa^2 - 1}{\kappa^2 + 1}, \qquad \Lambda = \frac{\lambda^2 - 1}{\lambda^2 + 1}.$$

Now, take the equations of motion for $\boldsymbol{n}_2$ and $\boldsymbol{n}_3$,

$$\begin{aligned}
\dot{\boldsymbol{n}}_2 &= \boldsymbol{\omega} \times \boldsymbol{n}_2 \\
&= \boldsymbol{\Omega} \times \boldsymbol{n}_2 + K\left(\boldsymbol{n}_1^{\mathrm{T}}\mathbb{S}\boldsymbol{n}_2\right)\boldsymbol{n}_1 + \frac{\Lambda - K}{K\Lambda - 1}\left(\boldsymbol{n}_2^{\mathrm{T}}\mathbb{S}\boldsymbol{n}_3\right)\boldsymbol{n}_3, \\
\dot{\boldsymbol{n}}_3 &= \boldsymbol{\omega} \times \boldsymbol{n}_3 \\
&= \boldsymbol{\Omega} \times \boldsymbol{n}_3 + \Lambda\left(\boldsymbol{n}_3^{\mathrm{T}}\mathbb{S}\boldsymbol{n}_1\right)\boldsymbol{n}_1 - \frac{\Lambda - K}{K\Lambda - 1}\left(\boldsymbol{n}_2^{\mathrm{T}}\mathbb{S}\boldsymbol{n}_3\right)\boldsymbol{n}_2.
\end{aligned}$$

The final step is to eliminate $\boldsymbol{n}_1$ from the equations. This elimination is accomplished by noting that

$$\mathbb{S}\boldsymbol{x} = (\boldsymbol{n}_1^{\mathrm{T}}\mathbb{S}\boldsymbol{x})\boldsymbol{n}_1 + (\boldsymbol{n}_2^{\mathrm{T}}\mathbb{S}\boldsymbol{x})\boldsymbol{n}_2 + (\boldsymbol{n}_3^{\mathrm{T}}\mathbb{S}\boldsymbol{x})\boldsymbol{n}_3,$$

implying

$$(\boldsymbol{n}_1^{\mathrm{T}}\mathbb{S}\boldsymbol{x})\boldsymbol{n}_1 = \mathbb{S}\boldsymbol{x} - (\boldsymbol{n}_3^{\mathrm{T}}\mathbb{S}\boldsymbol{x})\boldsymbol{n}_3 - (\boldsymbol{n}_2^{\mathrm{T}}\mathbb{S}\boldsymbol{x})\boldsymbol{n}_2.$$

Take the equation for $\dot{\boldsymbol{n}}_3$,

$$\begin{aligned}
\dot{\boldsymbol{n}}_3 &= \boldsymbol{\Omega} \times \boldsymbol{n}_3 + \Lambda\left(\boldsymbol{n}_3^{\mathrm{T}}\mathbb{S}\boldsymbol{n}_1\right)\boldsymbol{n}_1 - \frac{\Lambda - K}{K\Lambda - 1}\left(\boldsymbol{n}_2^{\mathrm{T}}\mathbb{S}\boldsymbol{n}_3\right)\boldsymbol{n}_2 \\
&= \boldsymbol{\Omega} \times \boldsymbol{n}_3 + \Lambda\left(\mathbb{S}\boldsymbol{n}_3 - (\boldsymbol{n}_3^{\mathrm{T}}\mathbb{S}\boldsymbol{n}_3)\boldsymbol{n}_3 - (\boldsymbol{n}_2^{\mathrm{T}}\mathbb{S}\boldsymbol{n}_3)\boldsymbol{n}_2\right) - \frac{\Lambda - K}{K\Lambda - 1}\left(\boldsymbol{n}_2^{\mathrm{T}}\mathbb{S}\boldsymbol{n}_3\right)\boldsymbol{n}_2 \\
&= \boldsymbol{\Omega} \times \boldsymbol{n}_3 + \Lambda\left(\mathbb{S}\boldsymbol{n}_3 - (\boldsymbol{n}_3^{\mathrm{T}}\mathbb{S}\boldsymbol{n}_3)\boldsymbol{n}_3\right) + \frac{K(1 - \Lambda^2)}{K\Lambda - 1}\left(\boldsymbol{n}_2^{\mathrm{T}}\mathbb{S}\boldsymbol{n}_3\right)\boldsymbol{n}_2.
\end{aligned}$$

In the same fashion, we find for $\dot{\boldsymbol{n}}_2$,

$$\dot{\boldsymbol{n}}_2 = \boldsymbol{\Omega} \times \boldsymbol{n}_2 + K\left(\mathbb{S}\boldsymbol{n}_2 - (\boldsymbol{n}_2^{\mathrm{T}}\mathbb{S}\boldsymbol{n}_2)\boldsymbol{n}_2\right) + \frac{\Lambda(1-K^2)}{K\Lambda-1}\left(\boldsymbol{n}_2^{\mathrm{T}}\mathbb{S}\boldsymbol{n}_3\right)\boldsymbol{n}_3.$$

In most places in this thesis, I write the cross product with $\boldsymbol{\Omega}$ as the matrix product with $\mathbb{O}$ instead. We also rename $\boldsymbol{n} = \boldsymbol{n}_3$ and $\boldsymbol{p} = \boldsymbol{n}_2$:

$$\dot{\boldsymbol{n}} = \mathbb{O}\boldsymbol{n} + \Lambda\left(\mathbb{S}\boldsymbol{n} - (\boldsymbol{n}^{\mathrm{T}}\mathbb{S}\boldsymbol{n})\boldsymbol{n}\right) + \frac{K(1-\Lambda^2)}{K\Lambda-1}\left(\boldsymbol{n}^{\mathrm{T}}\mathbb{S}\boldsymbol{p}\right)\boldsymbol{p},$$
$$\dot{\boldsymbol{p}} = \mathbb{O}\boldsymbol{p} + K\left(\mathbb{S}\boldsymbol{p} - (\boldsymbol{p}^{\mathrm{T}}\mathbb{S}\boldsymbol{p})\boldsymbol{p}\right) + \frac{\Lambda(1-K^2)}{K\Lambda-1}\left(\boldsymbol{n}^{\mathrm{T}}\mathbb{S}\boldsymbol{p}\right)\boldsymbol{n}$$

In terms of the aspect ratios λ and κ the equations read

$$\dot{\boldsymbol{n}} = \mathbb{O}\boldsymbol{n} + \frac{\lambda^2-1}{\lambda^2+1}\left(\mathbb{S}\boldsymbol{n} - \boldsymbol{n}^{\mathrm{T}}\mathbb{S}\boldsymbol{n})\boldsymbol{n}\right) + \frac{2\lambda^2(1-\kappa^2)}{(\lambda^2+\kappa^2)(\lambda^2+1)}(\boldsymbol{n}^{\mathrm{T}}\mathbb{S}\boldsymbol{p})\boldsymbol{p},$$
$$\dot{\boldsymbol{p}} = \mathbb{O}\boldsymbol{p} + \frac{\kappa^2-1}{\kappa^2+1}\left(\mathbb{S}\boldsymbol{p} - \boldsymbol{p}^{\mathrm{T}}\mathbb{S}\boldsymbol{p})\boldsymbol{p}\right) + \frac{2\kappa^2(1-\lambda^2)}{(\kappa^2+\lambda^2)(\kappa^2+1)}(\boldsymbol{n}^{\mathrm{T}}\mathbb{S}\boldsymbol{p})\boldsymbol{n}.$$

Part III
Papers

Paper A

Paper B

arXiv preprint available at http://arxiv.org/abs/1505.02661

Paper C

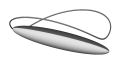

Paper D

arXiv preprint available at http://arxiv.org/abs/1508.04976

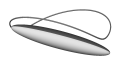

Paper E

arXiv preprint available at http://arxiv.org/abs/1503.03023

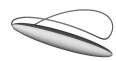

Paper F

arXiv preprint available at http://arxiv.org/abs/1412.3166